1985

I. A mechanistic study of the hydrodesulfurization of methanethiol over tungsten disulfide; II. A survey of rare earth sulfides for hydrodesulfurization activity

Donald Quinn Dowd
Iowa State University

INFORMATION TO USERS

This reproduction was made from a copy of a document sent to us for microfilming. While the most advanced technology has been used to photograph and reproduce this document, the quality of the reproduction is heavily dependent upon the quality of the material submitted.

The following explanation of techniques is provided to help clarify markings or notations which may appear on this reproduction.

1. The sign or "target" for pages apparently lacking from the document photographed is "Missing Page(s)". If it was possible to obtain the missing page(s) or section, they are spliced into the film along with adjacent pages. This may have necessitated cutting through an image and duplicating adjacent pages to assure complete continuity.

2. When an image on the film is obliterated with a round black mark, it is an indication of either blurred copy because of movement during exposure, duplicate copy, or copyrighted materials that should not have been filmed. For blurred pages, a good image of the page can be found in the adjacent frame. If copyrighted materials were deleted, a target note will appear listing the pages in the adjacent frame.

3. When a map, drawing or chart, etc., is part of the material being photographed, a definite method of "sectioning" the material has been followed. It is customary to begin filming at the upper left hand corner of a large sheet and to continue from left to right in equal sections with small overlaps. If necessary, sectioning is continued again—beginning below the first row and continuing on until complete.

4. For illustrations that cannot be satisfactorily reproduced by xerographic means, photographic prints can be purchased at additional cost and inserted into your xerographic copy. These prints are available upon request from the Dissertations Customer Services Department.

5. Some pages in any document may have indistinct print. In all cases the best available copy has been filmed.

University
Microfilms
International
300 N. Zeeb Road
Ann Arbor, MI 48106

Dowd, Donald Quinn

I. A MECHANISTIC STUDY OF THE HYDRODESULFURIZATION OF METHANETHIOL OVER TUNGSTEN-DISULFIDE. II. A SURVEY OF RARE EARTH SULFIDES FOR HYDRODESULFURIZATION ACTIVITY

Iowa State University PH.D. 1985

I. A mechanistic study of the hydrodesulfurization of methanethiol over tungsten disulfide

II. A survey of rare earth sulfides for hydrodesulfurization activity

by

Donald Quinn Dowd

A Dissertation Submitted to the
Graduate Faculty in Partial Fulfillment of the
Requirements for the Degree of
DOCTOR OF PHILOSOPHY

Department: Chemistry
Major: Physical Chemistry

Approved:

Signature was redacted for privacy.

In Charge of Major Work

Signature was redacted for privacy.

For the Major Department

Signature was redacted for privacy.

For the Graduate College

Iowa State University
Ames, Iowa

1985

TABLE OF CONTENTS

GENERAL INTRODUCTION

This thesis describes a research effort in two areas of catalytic hydrodesulfurization; the search for rare earth sulfides for an alternative catalyst and the establishment of detailed reaction kinetics. The original intent of the project was to use the most active rare earth sulfide for the kinetic study, but this study was performed using tungsten disulfide as the catalyst when it was ascertained that the activity of the most active rare earth sulfide was insufficient for the type of kinetic study envisioned.

As an organizational convenience, this thesis has been separated into two parts; the first pertains to the kinetics of the hydrodesulfurization, HDS, reaction and the second deals with the testing of the rare earth sulfides for HDS catalytic activity.

PART I. A MECHANISTIC STUDY OF THE HYDRODESULFURIZATION OF METHANETHIOL OVER TUNGSTEN DISULFIDE.

INTRODUCTION

Hydrodesulfurization, HDS, is the hydrogenolysis of organosulfur compounds to hydrogen sulfide and hydrocarbons. Early incentives for this sulfur removal centered around the industrial processing of petroleum (1), e.g., to eliminate corrosion in the reforming process and to improve burning characteristics. More recently (2), the concern about air quality has shifted the incentive to eliminating the sulfur prior to its combustion to sulfur dioxide.

The industrial process, conducted at 575-725 K and 50-200 atm (3), uses a catalyst commonly referred to as "cobalt molybdate", although nickel and tungsten may replace the cobalt and molybdenum. The catalyst is prepared by impregnation of a high area γ-alumina support with cobalt nitrate and ammonium molybdate. The catalyst is then dried, calcined and finally sulfided either by pretreatment or during the course of the HDS reaction. Molybdenum, in the absence of cobalt, is quite active while the converse is not true (4,5). The addition of cobalt enhances the HDS activity, which exhibits a peak in the range Co/(Co+Mo) =.2-.45 (6-10). In addition to hydrodesulfurization, these catalysts are also good hydrogenation, HYD, catalysts and are therefore bifunctional in nature.

Correlations between activity and concentration of a particular structural component of the catalyst are used to identify the catalytically active phase. These phases are generally identified by their X-ray diffraction patterns. The absence of such patterns for normal HDS catalysts has focused much of the recent HDS research toward identifying the active phase or phases. Several articles (11-15) have recently reviewed the structural aspects of these catalysts.

The early lack of evidence for bulk Mo, Co, or Mo-Co sulfide phases led to several proposals regarding the nature of the active phase. These proposals are often used as the framework for reviewing structural studies and will be used similarly here. All the models agree on an essentially monolayer dispersion of molybdenum oxide, which bonds to the alumina by replacing the existing hydroxyl groups. This oxide or calcined state is often referred to as the precursor state. There is some debate about the distribution of the Co in the precursor state, but it is generally accepted that some is located in the alumina whereas the remainder of the cobalt is either associated with the Mo layer or present as bulk Co_3O_4 (11-16).

The models diverge with regard to the effect of sulfidation and the specifics regarding the active Co phase. The monolayer model (15,17) assumes a partial replacement of

the terminal oxygen anions with sulfur while maintaining the precursor's monolayer configuration. The active Co is intimately associated with active Mo sites (15) but the exact manner of promotion or location of the Co has not been described. The intercalation model (18-20) assumes the Mo monolayer undergoes complete sulfidation to microcrystallites of MoS_2 having a layered structure similar to bulk MoS_2. The cobalt active in promotion is intercalated at the edges between MoS_2 layers and either increases or stabilizes the number of active sites. The synergism or junction model (21,22) proposes separate microcrystals of MoS_2 and Co_9S_8. The promoting effect of Co occurs at the contact points between these two phases, possibly due to a hydrogen-spillover effect (23).

The monolayer model suggests incomplete sulfidation, i.e., formation of the thermodynamically stable MoS_2 and Co_9S_8 phases does not occur. In its original form (17), the model viewed the precursor state as two dimensional oxide islands. Sulfidation then replaces the top oxygen anion layer with sulfur to give a sulfur-to-molybdenum ratio of one (one sulfur anion replaces two oxygen anions for steric reasons). Observed S:Mo ratios much larger than 1:1 led Massoth (24) to describe the precursor and sulfided states as one-dimensional chains instead of two-dimensional

islands. The separation between the one-dimensional chains is such that two sulfurs can coordinate to each molybdenum; hence the observed 2:1 ratio. The proponents of the monolayer model suggested that the spectroscopic results, while suggestive of a MoS_2 phase, did not rule out a MoO_xS_y species (25).

Recently the use of EXAFS, which probes the local environment about an atom, has shown that the first coordination sphere about Mo consists entirely of sulfur (26-28), the sulfur-to-molybdenum coordination number approaching 6 as in MoS_2. This identification of the sulfided molybdenum as MoS_2 agrees with the bulk of the spectroscopic data (11) and rationalizes the similarity in behavior when unsupported MoS_2 and supported catalysts are impregnated with cobalt (14,29). The high dispersion of this sulfide phase (30,31) suggests that two-dimensional (i.e., a single "sandwich" layer) MoS_2 islands or chains are formed in the sulfidation process and not the three-dimensional MoS_2 particles postulated in the intercalation model.

While the molybdenum is located in a two-dimensional MoS_2-like structure, cobalt is distributed between three phases; in the alumina support, as bulk Co_9S_8 and in association with the surface MoS_2 (13,14,32). Topsøe

et al. (33,34) using Mossbauer Emission Spectroscopy, MES, in conjunction with activity measurements have identified the last phase, referred to as Co-Mo-S, as the active component in supported and unsupported catalysts. Although the location of cobalt in this phase has not been established, Topsøe currently places it at the edge of the MoS_2 platelets. No correlation was observed between Co_9S_8 and catalytic activity as hypothesized in the synergism model.

Although none of the original models was totally correct, they did provide a starting point for structural studies. These studies have led to the current view of molybdenum in the form of highly dispersed MoS_2-like islands or chains. The active cobalt is associated with this MoS_2, although its exact location and manner of promotion is unclear.

In addition to the structural studies just mentioned, activity measurements are performed in order to develop kinetic expressions and reaction pathways that describe the HDS process. The model compounds most frequently used are heteroatomic aromatics (thiophenes): thiophene, benzothiophene and dibenzothiophene. Although, as a class, these are the least reactive, they are also the most prevalent organosulfur compounds found in the heavier feedstocks

currently being introduced and are therefore viewed as better analogs for the actual industrial HDS process. The relative reactivities in HDS (35) are:

thiols (mercaptans) > disulfides > sulfides > thiophenes

While the activity data and "best fit" rate expressions using different thiophenic compounds, catalyst compositions, reactor systems and experimental conditions are not entirely consistent, a few generalizations can be made (36):

1) Limiting positive orders of +1 have been observed for both reactants (37-40), although orders of +1/2 have been reported for H_2 (41-43).

2) Reactant inhibition, shifting positive orders from +1 toward zero, with changing pressure or temperature have been seen for both reactants (40,44), although H_2 inhibition is rarely investigated.

3) Significant reaction inhibition occurs in the presence of H_2S (37,45), whereas contradictory evidence regarding hydrocarbon inhibition has been reported (36).

4) HDS involves a surface reaction between adsorbed organosulfur compound and adsorbed hydrogen.

5) A dual site mechanism has been suggested, with one site for hydrogen adsorption and another where the organosulfur compound and H_2S adsorb.

The above statements themselves can be generalized into a rate expression of the form:

$$\text{rate} = k \cdot \frac{K_S P_S}{(1+K_S P_S+\Sigma K_i P_i)^n} \cdot \frac{[K_H P_H]^m}{(1+[K_H P_H]^m)^p} \qquad \text{(I-1)}$$

where k is the rate constant, the subscripts S, H and i signify the organosulfur compound, hydrogen and reaction products respectively, K and P represent the adsorption constant and pressure of the gas phase species, m is the hydrogen order, and n and p are the order dependencies for the thiophenic and hydrogen denominators. Depending on the limiting positive hydrogen order seen, m is either +1 or +1/2. When hydrogen inhibition is observed (i.e., a hydrogen order between zero and +1) the proposed rate expression includes the hydrogen denominator (p=1, which does not imply a negative hydrogen order at high hydrogen pressures), whereas it is often neglected by those who do not observe inhibition by hydrogen (p=0). The thiophenic inhibition order, n, is reported as both 1 and 2. Vrinat (36) has noted that the value of two is commonly reported when the hydrogen inhibition term is neglected, p=0. It should be noted that a n=2 value suggests a negative limiting order at high thiophenic pressures. This has not been observed, whereas a zero order dependency, n=1, has been seen (45).

The interpretation of the proposed rate expressions just described assumes a dual site mechanism where hydrogen

adsorbs to the sulfur of the catalyst and gas phase sulfur containing compounds adsorb at a single edge sulfur vacancy. In addition to this interpretation, sulfur adsorbing and reacting at two independent sites (32) and a sulfur adsorption site consisting of more than one vacancy (46) have been proposed.

The bifunctional nature of cobalt-molybdate catalysts, hydrodesulfurization and hydrogenation activity, increases the number of possible reaction products seen in thiophenic desulfurization. The distribution of these products has been used to develop schemes that outline the sequence of surface reaction intermediates. These schemes are not meant to be mechanisms on a molecular scale and Zdrazil (47) has recently questioned the interpretation of the presence of a product in the gas phase in terms of its importance as a surface reactive intermediate. Nevertheless, they are frequently used in the literature and Figure I-1 shows such a scheme for thiophene HDS (32). The identification of butadiene (48) and tetrahydrothiophene (49), at higher conversions and H_2 pressures respectively, in the gas phase has led to an acceptance of both ring hydrogenation (upper pathway in Figure I-1) and sulfur extraction (lower pathway in Figure I-1) as first steps in the reaction network. Similar dual pathways have been proposed for benzothiophene

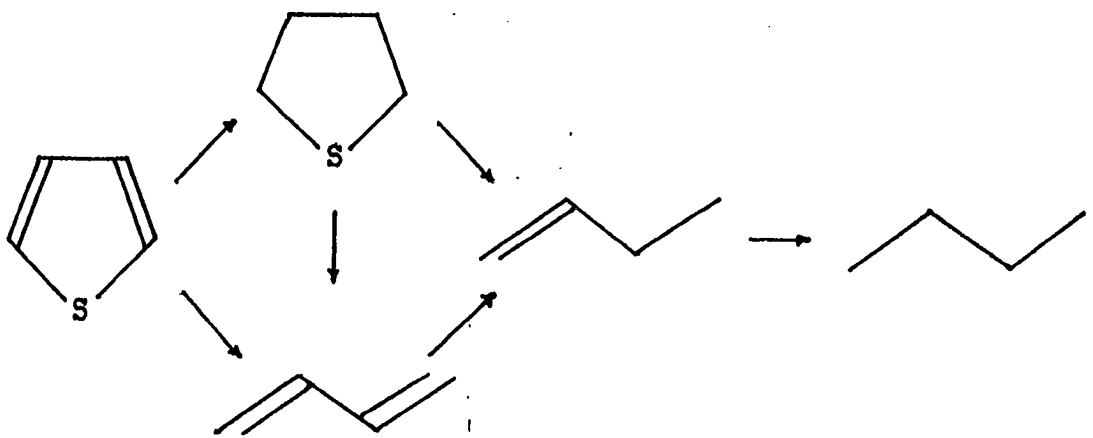

Figure I-1. Reaction network for thiophene HDS (From Massoth and MuraliDhar [32])

(50) and dibenzothiophene (51). Based primarily on poisoning studies (32), the HYD and HDS reactions are thought to occur on different sites.

The first step in any mechanism is the adsorption of reactants. The kinetic studies mentioned above conclude that there are separate sites for the sulfur containing species and hydrogen. The adsorption of H_2S and organosulfur compounds can be viewed as processes analogous to sulfidation: formation of sulfur-metal bonds via adsorption at a sulfur (anion) vacancy. HDS inhibition by H_2S would then be explained by the competitive adsorption of H_2S and organosulfur species on the same site. Exchange of surface sulfur with gas phase sulfur during H_2S adsorption and HDS reaction studies (52,53) can also be rationalized in this manner.

These vacancies are usually assumed to be located at the edges of the MoS_2 particle where the sulfur anion is coordinated to the fewest metal atoms. Stevens and Edmonds (54) reported higher activities for unsupported MoS_2 with larger basal/edge area ratios, although serious questions have been raised about this interpretation (55). Since the edges of a MoS_2 single crystal oxidize more readily than the basal plane (56), Tauster et al. (57) have suggested that oxygen selectively chemisorbs at the edges. Linear

relationships between activity and the dissociative adsorption of O_2 have been observed (57-59). A similar linear relationship has been seen for NO adsorption (60). NO adsorbs as a dimer and Valyon and Hall (61) have speculated that adjacent vacancies on the same metal atom are required for dimeric adsorption. It should be noted that these linear relationships are not always seen (62-64).

The actual form of molecularly adsorbed thiophene is unclear. Desulfurization without ring hydrogenation is often cited as evidence for through sulfur adsorption, whereas the converse is cited to support π-type adsorption through the ring. Steric inhibition being less than anticipated for methyl substitutions α to the sulfur has also been cited as evidence for adsorption parallel to the surface (65). Kilanowski et al. (66) have suggested that a number of vacancies may be needed for π-ring adsorption and only one vacancy for through sulfur (perpendicular) adsorption. Since the number of vacancies is related to H_2 pressure (via sulfur removal as H_2S), this could explain the different reactivity-organosulfur structure patterns observed at different H_2 pressures (66). Kwart et al. (67) have speculated that π adsorption may not involve the entire ring but only one π-bond or one π-bond and the sulfur heteroatom.

Hydrogen adsorption is usually described as occurring on the sulfur of MoS_2. Dissociative adsorption yielding sulfhydril groups has been seen using Inelastic Neutron Scattering, INS (68,69). Titration of these S-H groups correlates with HDS activity suggesting their involvement in the reaction (70). Schuit (20) has speculated that this dissociative adsorption might be heterolytic and similar to that observed for hydrogen on ZnO (71,72):

$$H_2 + S + * \langle===\rangle HS + H* \qquad (I-2)$$

$$H* + S \langle===\rangle HS + * \qquad (I-3)$$

where S is a surface sulfur and * is a vacancy. In a similar proposal, Fraser et al. (73) suggest the initial adsorption step only involves hydrogen bonding to the exposed metal and sulfhydril formation occurs in subsequent slow atomic hydrogen migration steps. This proposal, which does not state whether the initial hydrogen adsorption step is molecular or dissociative, is based on their observation that H_2-D_2 exchange does not involve sulfhydril hydrogen. INS evidence is inconclusive on the existence of a metal-hydrogen bond (74). H_2S inhibition of the exchange reaction (75) supports Fraser's proposal that some type of hydrogen-metal interaction is occurring. Although dissociative adsorption of H_2 is accepted, the first order HDS rate

dependence on H_2 is often interpreted to mean a molecular hydrogen species is involved in the reaction.

Step by step mechanisms are rare. The lack of a consensus concerning the form of thiophenic adsorption and whether ring hydrogenation or cleavage of the carbon-sulfur bond occurs first are the probable reasons for this deficiency. Since the primary object of hydrodesulfurization is carbon-sulfur bond scission, it is not inappropriate to avoid these issues by studying a simpler class of organosulfur compounds, e.g., thiols.

Williamson et al. (46), Wilson et al. (75), Kieran and Kemball (76) and Wilson and Kemball (77) have studied the desulfurization of methanethiol and ethanethiol over MoS_2 and WS_2. Even with these simpler molecules competing reactions are present. For ethanethiol, the following reactions were observed:

$$2\ C_2H_5SH \langle===\rangle (C_2H_5)_2S + H_2S \qquad (I\text{-}4)$$

$$C_2H_5SH \langle===\rangle C_2H_4 + H_2S \qquad (I\text{-}5)$$

$$H_2 + C_2H_5SH \langle===\rangle C_2H_6 + H_2S \qquad (I\text{-}6)$$

Under the same reaction conditions, Kieran and Kemball (76) observed that the desulfurization reactions of ethyl sulfide, equations I-7 through I-9, occurred at roughly one-

$$(C_2H_5)_2S \leftrightarrows 2C_2H_4 + H_2S \quad \text{(I-7)}$$

$$H_2 + (C_2H_5)_2S \leftrightarrows C_2H_4 + C_2H_6 + H_2S \quad \text{(I-8)}$$

$$2H_2 + (C_2H_5)_2S \leftrightarrows 2C_2H_6 + H_2S \quad \text{(I-9)}$$

fifth the rate of ethanethiol desulfurization (equations I-4 through I-6), with equation I-7 the primary ethyl sulfide desulfurization pathway. Methanethiol and methyl sulfide exhibit behavior analogous to equations I-4, I-6 and I-9. Using the temperatures at which these reactions and those for deuterium exchange are first observed, the following order of bond activation (ease of bond scission) was ascertained for MoS_2.

H-H > S-H > C-S, C-H(C_2 compound) > C-H(C_1 compound) >> C-C

The same sequence was observed for WS_2 but with greater relative differences.

A recent study of ethanethiol HDS with deuterium has led Williamson et al. to refer to the active site as a triply coordinatively unsaturated metal atom, i.e., a metal atom with three vacancies (46). Although a detailed proposal was not presented, an argument similar to that used by Tanaka and Okuhara (78) to explain exchange and/or hydrogenation of olefins over MoS_2 was suggested.

The experimental measurements of the HDS reaction rate have generally been analyzed using the Langmuir-Hinshelwood kinetic formalism. One manifestation of this formalism is that the rate displays varying pressure dependencies for the reactants and those products that adsorb (e.g., the reactant pressure dependency may change from first order to zeroth or negative first order with increasing reactant pressure). Such pressure dependencies have been partially investigated for the organosulfur reactant but only superficially examined for the hydrogen reactant and product gases. This inattention has resulted in some disagreement regarding the denominator of the rate expression (see the discussion concerning the generalized rate expression, equation I-1). The use of heteroaromatic sulfur compounds in these studies, which undergo partial hydrogenation in addition to desulfurization, has also directed attention away from the fundamental processes involved in breaking the carbon-sulfur bond and to the question of when this hydrogenation occurs. The aim of this study is to more fully explore the pressure dependencies of the reactant and product gases and to focus on the carbon-sulfur bond breaking process. This was achieved using a simple model system, equation I-10, with

$$CH_3SH + H_2 \xrightarrow[WS_2]{} CH_4 + H_2S \qquad \text{(I-10)}$$

methanethiol as the organosulfur reactant and WS_2 and the catalyst. Unsupported WS_2 was used as the catalyst since side reactions, analogous to equation I-4, are less of a problem with WS_2 than MoS_2.

EXPERIMENTAL

Apparatus

The large variations in partial and total pressures envisioned in this study are most easily attained using a low vacuum apparatus. A schematic of the system is shown in Figure I-2. The system, constructed of pyrex and stainless steel, can be divided into two parts. The first section, unshaded, contains a quadrupole mass spectrometer and ion pump. This section has a base pressure of 1×10^{-7} Pa (ultra high vacuum, UHV) and is pumped by two 2-stage mercury diffusion pumps in series. These pumps were separated from the UHV by a liquid nitrogen (LN_2) trap and backed by a LN_2 trapped single-stage rotary vane pump. The second section, the reaction chamber (shaded), contains a gas manifold, two capacitance manometers and the catalyst vessel. The reaction chamber and reference sides of the capacitance manometers, base pressures $\sim 1 \times 10^{-4}$ Pa (high vacuum, HV), were each pumped by a LN_2 trapped 2-stage mercury diffusion pump. Both diffusion pumps were backed by the same LN_2 trapped single stage rotary vane pump. HV and UHV pressure measurements were obtained using Bayard-Alpert ionization gauges suitable in the presure range 0.1 - 1×10^{-8} Pa.

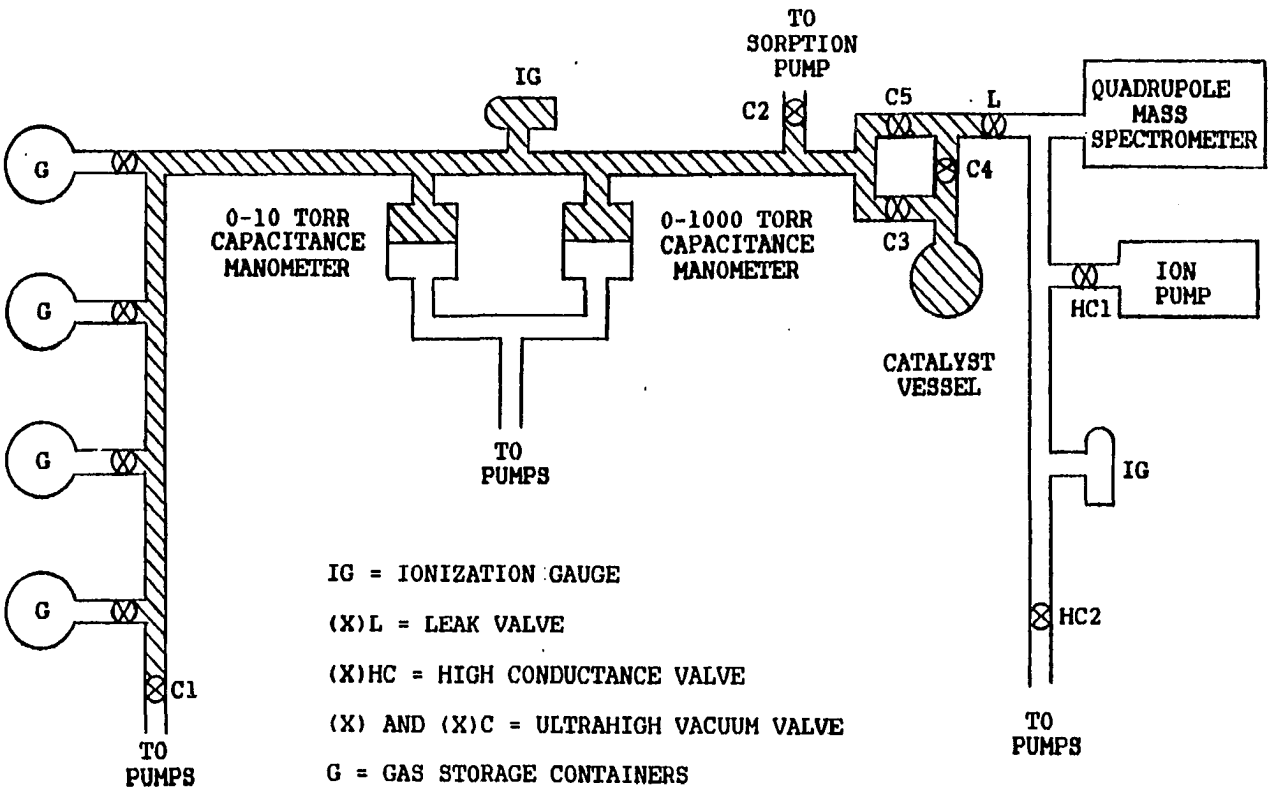

Figure I-2. Schematic of the experimental apparatus

Reaction chamber pressures in the range of .133 - 1.33 x 10^3 Pa (1 x 10^{-3} - 10 Torr) were measured using the "low pressure" (10 Torr) capacitance manometer (Granville Phillips Co., series 212) after calibration against a McLeod gauge (Consolidated Vacuum Corporation, Type GM 100A) using nitrogen gas. Linear calibration curves were obtained. Scale readings were read from a digital multimeter (Hewlett-Packard, series 3465A). The sensor head was water thermostated to 306.4 K to avoid drift due to ambient temperature changes.

A "high pressure" (1000 Torr) capacitance manometer (MKS Instruments, Type 107M-315BH-1000) was used for pressures greater than 1.33 x 10^3 Pa (10 Torr). The manometer was factory calibrated and this calibration was used after it was checked for accuracy. The sensor head was thermostated at ~318 K using an aluminum block heater (MKS, Type 170M-39). Pressures were read from a digital multimeter (Hewlett-Packard, series 3465A).

The catalyst vessel, a 500-ml pyrex round bottom flask connected to a 2 3/4 inch conflat flange, was heated using a tube furnace (S. B. Lindberg, Type SP) covered at both ends to prevent air flow through the furnace. The temperature was monitored using a chromel-alumel thermocouple inside the furnace and in direct thermal contact with the catalyst

vessel. Temperature readings were obtained using a digital readout meter (Omega Engineering, Model 199) and were stable within ±2 K after thermal equilibrium was attained.

A quadrupole mass spectrometer (Finnegan Corp., Model 400) was used to monitor the gas phase composition in the reaction chamber. A current amplifier (Keithley, Model 427) was used to amplify the spectrometer output by a factor of 1 x 10^8 volts/ampere prior to recording the output, in millivolts, on a two-channel oscillographic recorder (Hewlett-Packard, Model 7402A). The mass spectrometer sensitivities, S_i= gas pressure (Pa)/signal (mv), were determined by calibrating this recorder output against the actual pressure in the manifold (for a particular leak valve setting). These sensitivities were constant to within ~ ±5%. A reliable sensitivity factor for methanethiol was not obtained due to slow attainment of equilibrium across the leak valve. An oscilloscope (Tektronix Inc., Type RM503) was used in conjunction with the oscillographic recorder for troubleshooting and instrument adjustment.

Kinetic Procedure

Hydrodesulfurization of methanethiol over WS_2 was studied at 623 K. 6.17 grams of WS_2 were placed in the catalyst vessel, evacuated to ~1.33 x 10^{-4} Pa (10^{-6} Torr)

and underwent a once only pretreatment of 1.27×10^3 Pa (9.5 Torr) H_2S at 653 K for ~90 minutes. The normal preparation between runs consisted of two ten-minute exposures to 1.33×10^3 Pa (10 Torr) of hydrogen, a 1.33×10^2 Pa (1 Torr) exposure to H_2S for five minutes and a 1.33×10^3 Pa (10 Torr) flush of H_2, all at reaction temperature. The mass spectrometer was isolated from the reaction chamber during the H_2S exposure and H_2 flush (valves C_4 and C_5 are closed and valve L remains open).

For a catalytic run, the reaction chamber was evacuated to less than 2.66×10^{-2} Pa (2×10^{-4} Torr) and the catalyst vessel isolated (valves C_3 and C_5 are closed and valves C_4 and L are open). The leak valve, L, was set at a position that let the apparatus operate as a batch reactor and remained at this setting for all experiments. The appropriate gas mixture was then dosed into the manifold (reaction chamber minus the catalyst vessel) with the pressures being read by the capacitance manometer. The catalyst was exposed to the gas mixture by opening valve C_3. The reaction was monitored by using the mass spectrometer to follow product (usually methane) formation. Initial rates were determined using the following equation

$$\text{rate} = [\Delta mv/\Delta t] \times S_i(\text{Pa/mv})$$

where [$\Delta mv/\Delta t$] is the change in recorder signal (millivolts) with time and S_i is the mass/charge (m/z) sensitivity factor for product gas i. The rate was converted to molecules/($cm^2 \cdot sec$) by dividing the above rate by the surface area of the catalyst and using the ideal gas law to convert from Pascals to molecules. This conversion factor, C, was determined using the following expression:

$$C = \frac{N_A \cdot P'}{R \cdot A} \cdot \left(\frac{V}{T} + \frac{V'}{T'} \right)$$

Since only a fraction of the reaction chamber volume was at reaction temperature, the volume and temperature terms have two components. N_A is Avogadro's number, P' the conversion factor from Pascals to atmospheres (9.868×10^{-6} atm/Pa), R is the gas constant (0.0821 L·atm/K·mole), A is the surface area of the catalyst (1.46×10^5 cm^2), V the volume of the reaction chamber at room temperature (1.82 L), T equals room temperature (295 K), V' is the reaction volume at reaction temperature (.54 L), and T' is the reaction temperature (typically 623 K). For a reaction temperature of 623 K, the conversion factor is 3.498×10^{12} molecules/($cm^2 \cdot Pa$).

Four types of reaction mixtures were dosed into the reaction chamber:

1) Constant hydrogen and variable methanethiol pressures for determination of the methanethiol rate dependency.

2) Constant methanethiol and variable hydrogen pressures for determination of the hydrogen rate dependency.

3) Constant methanethiol/hydrogen and variable hydrogen sulfide pressures for determination of hydrogen sulfide product inhibition.

4) Constant methanethiol/hydrogen and variable methane pressures for determination of methane product inhibition.

Methane production was monitored in all runs except those of methane inhibition, where hydrogen sulfide production was monitored.

The mass spectrometer cracking patterns of methanethiol overlapped the patterns of both methane and hydrogen sulfide. Reducing the ionization energy to 35 volts, emission current ~1 milliamp, made a simple subtraction procedure for m/z=16 (methane) feasible. The problem was more severe for hydrogen sulfide except at low thiol pressures and moderate-to-high rates.

An additional difficulty in following the reaction with hydrogen sulfide was the existence of the disproportionation reaction at high thiol pressures

$$2\ CH_3SH \langle===\rangle (CH_3)_2S + H_2S \qquad (I\text{-}11)$$

No disproportionation was observed for hydrogen to thiol ratios greater than 12.5:1. Even at its largest rate less than 1% of the thiol is consumed in the reaction.

The methane inhibition runs required following the production of hydrogen sulfide (m/z=34). To avoid H_2S production due to disproportionation, an ~60:1 hydrogen to methanethiol ratio, with a low mercaptan pressure, was used. The low mercaptan pressure also minimized the methanethiol-hydrogen sulfide overlap, permitting a simple subtraction process to be used.

Materials

The gases used in all experiments, except hydrogen, were transferred from lecture bottles to glass bulbs attached to the system. The methanethiol (Linde, 99.5%), hydrogen sulfide (Matheson, 99.5%), and methane (Matheson, 99.97%) were used after undergoing repeated freeze-pump-thaw-freeze purification cycles using LN_2. Hydrogen (Air Products, hydrogen zero, 99.95%) was used straight from the cylinder after the line to the cylinder valve underwent repeated evacuations and pressurizations.

The B.E.T. surface area (Micrometrics Instruments Corp., model 2100D) of the WS_2 (CERAC, Lot #5264) was 2.36 m^2/g. The manufacturer's certificate of analysis indicated an average particle size of .90 microns and the per cent composition of 74.06 (theoretical 74.14) and 25.86 (theoretical 25.86) for tungsten and sulfur respectively.

RESULTS AND DISCUSSION

The aim of these experiments is to determine the relationship between the pressure of each reactant and product gas and the rate of methanethiol hydrodesulfurization. The results of these experiments are shown in Figures I-3 through I-8 in a $\log_{10}$(rate) versus $\log_{10}$ (pressure) form. The solid lines are provided as references for possible limiting order dependencies.

The reaction rate as a function of methanethiol pressure, at a constant hydrogen pressure of 1.777×10^3 Pa (13.33 Torr) and catalyst temperature of 623 K, is shown in Figure I-3. The thiol dependence is nearly first order at low partial pressures, and at larger partial pressures this shifts toward a negative first order dependence. Such a shift is typically associated with surface reactions where two or more of the reactants compete for the same type of site. Additional, less complete, pressure dependencies are shown in Figures I-4a and I-4b. These dependencies were obtained for constant hydrogen pressures of 4.263×10^3 Pa (31.97 Torr) and 5.685×10^3 Pa (42.64 Torr) respectively and a catalyst temperature of 623 K.

The reaction rate as a function of hydrogen pressure, at a constant methanethiol pressure of 31.5 Pa (0.236 Torr) and temperature of 623 K, is shown in Figure I-5. Again the

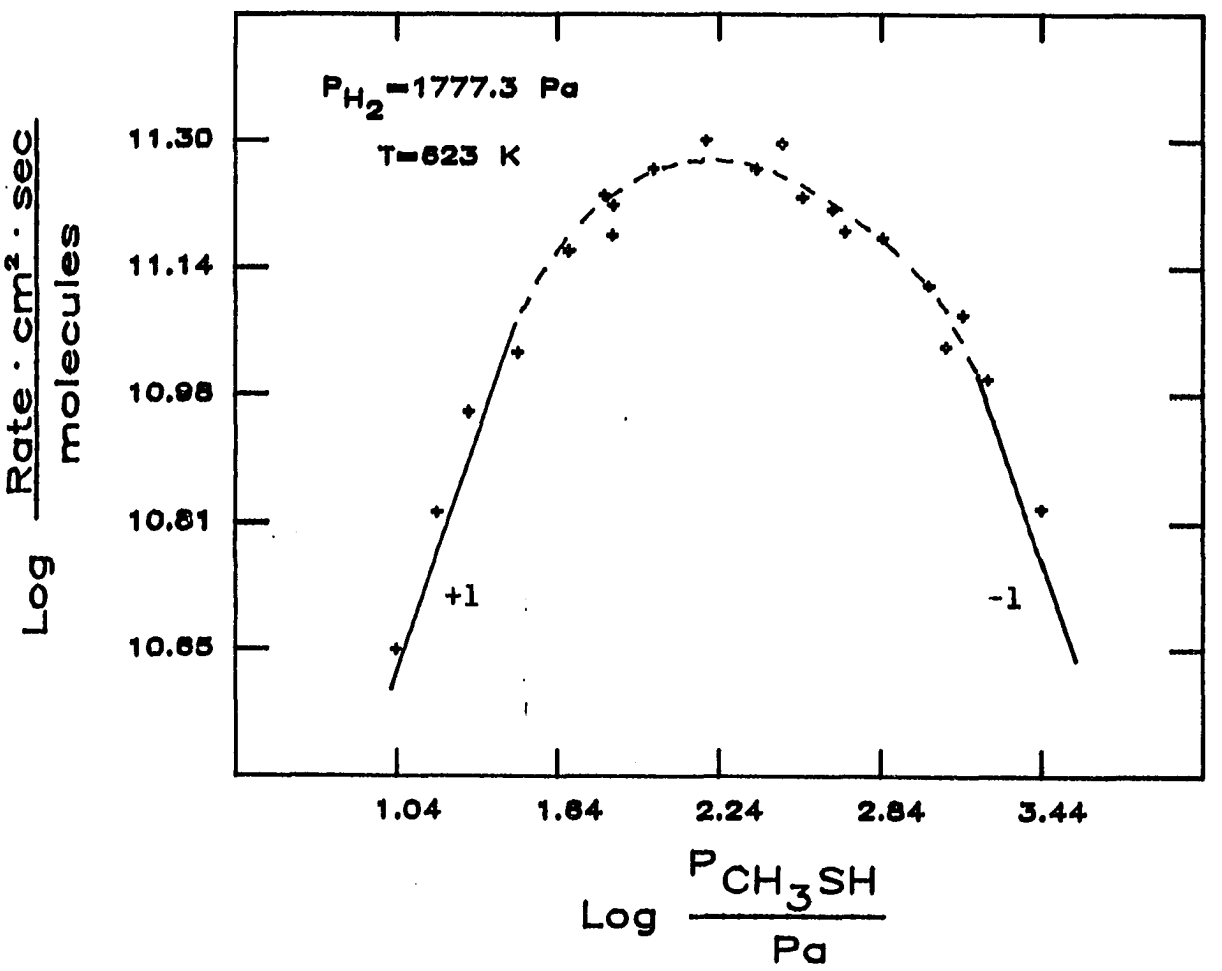

Figure I-3. Methanethiol order plot (623 K) at a constant hydrogen pressure of 1777.3 Pa. The solid lines represent possible limiting pressure order dependencies

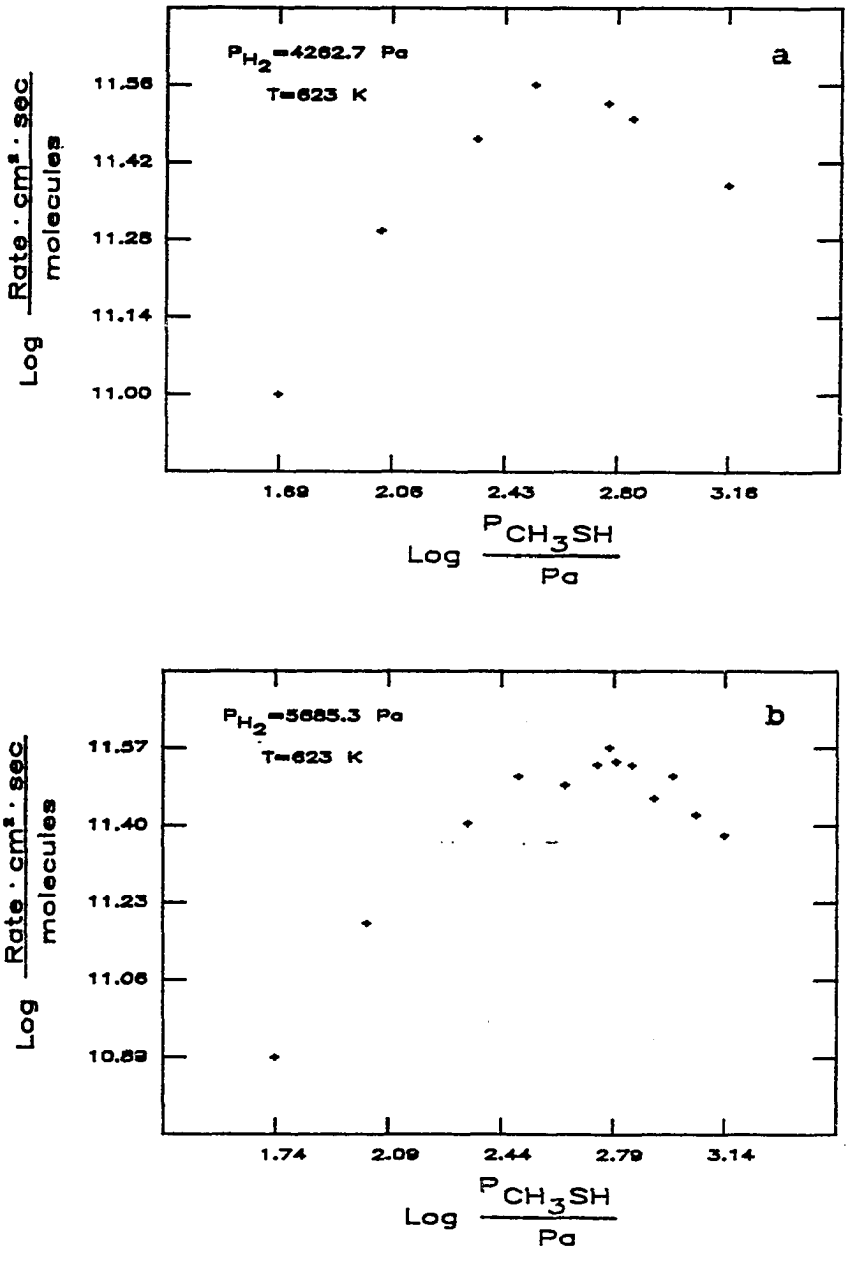

Figure I-4. Methanethiol order plots (623 K) at a constant hydrogen pressure of 4262.7 Pa (a) and 5685.3 Pa (b)

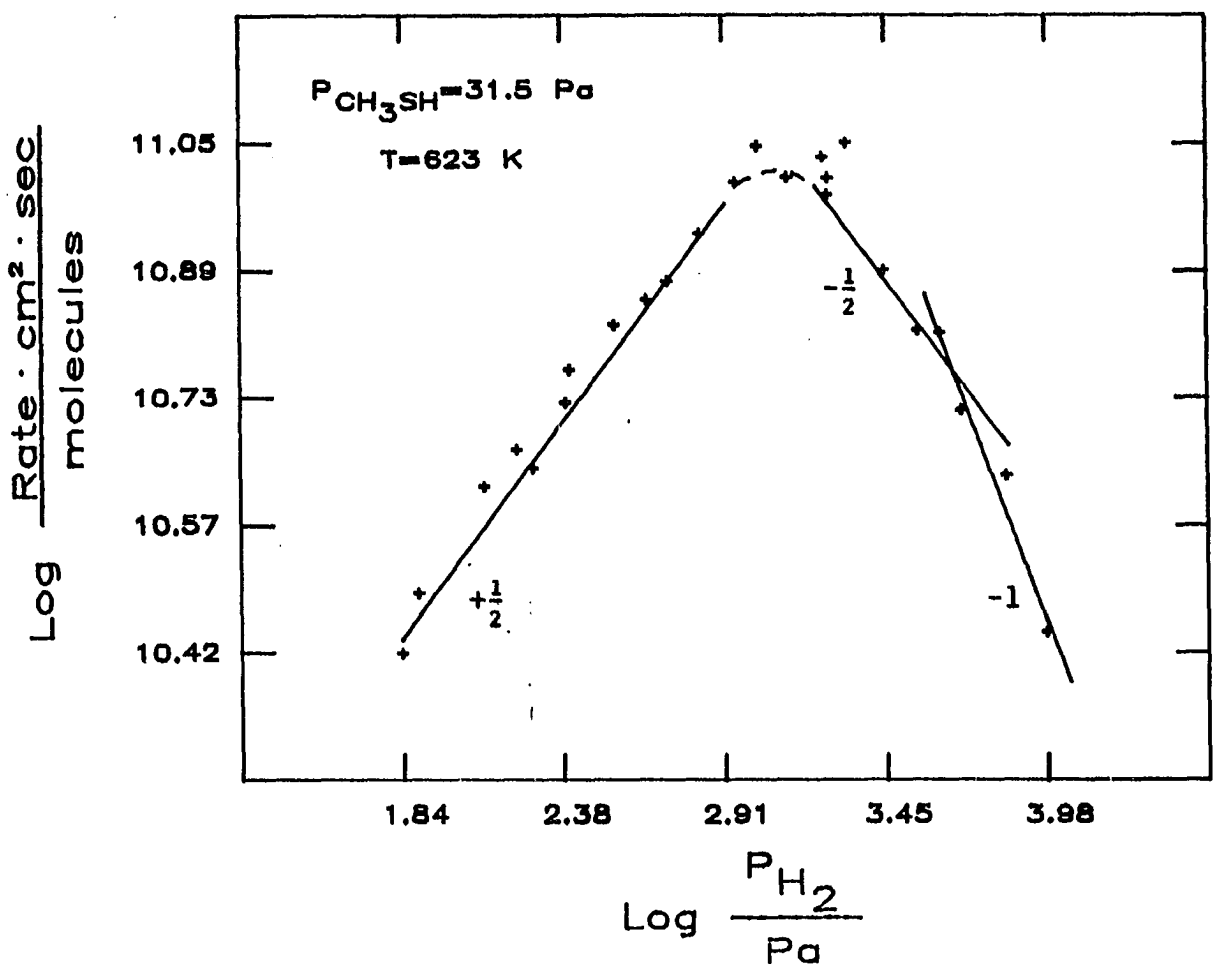

Figure I-5. Hydrogen order plot (623 K) at a constant methanethiol pressure of 31.5 Pa. The solid lines represent possible limiting pressure order dependencies

pressure dependency shows a shift from a positive (+1/2) to a negative (-1/2 or -1) order and is suggestive of a rate limiting surface reaction. Additional partial pressure dependencies are shown in Figures I-6a and I-6b. These dependencies were obtained at a catalyst temperature of 623 K and constant methanethiol pressures of 70.3 Pa (.527 Torr) and 1.059×10^2 Pa (.794 Torr) respectively.

Figures I-7 and I-8 show the product order dependencies for methane and hydrogen sulfide. These data were taken at constant reactant pressures of 1.777×10^3 Pa (13.33 Torr) of hydrogen and 31.5 Pa (0.236 Torr) of methanethiol and catalyst temperature of 623 K. Initially, a zero order dependency is observed for both products that shifts to orders of -1 and -1 to -2 at much larger pressures of methane and hydrogen sulfide respectively. The reactant rate data were determined in the pressure range where zero order dependencies were observed for the two products.

Any mechanistic description of these results must incorporate factors relating to the adsorption process, the dominant surface species, and the structure of the catalyst. The interrelationship between these aspects of the HDS process is easily presented in the context of a rate expression. For this purpose the generalized rate expression described earlier will be used. While this

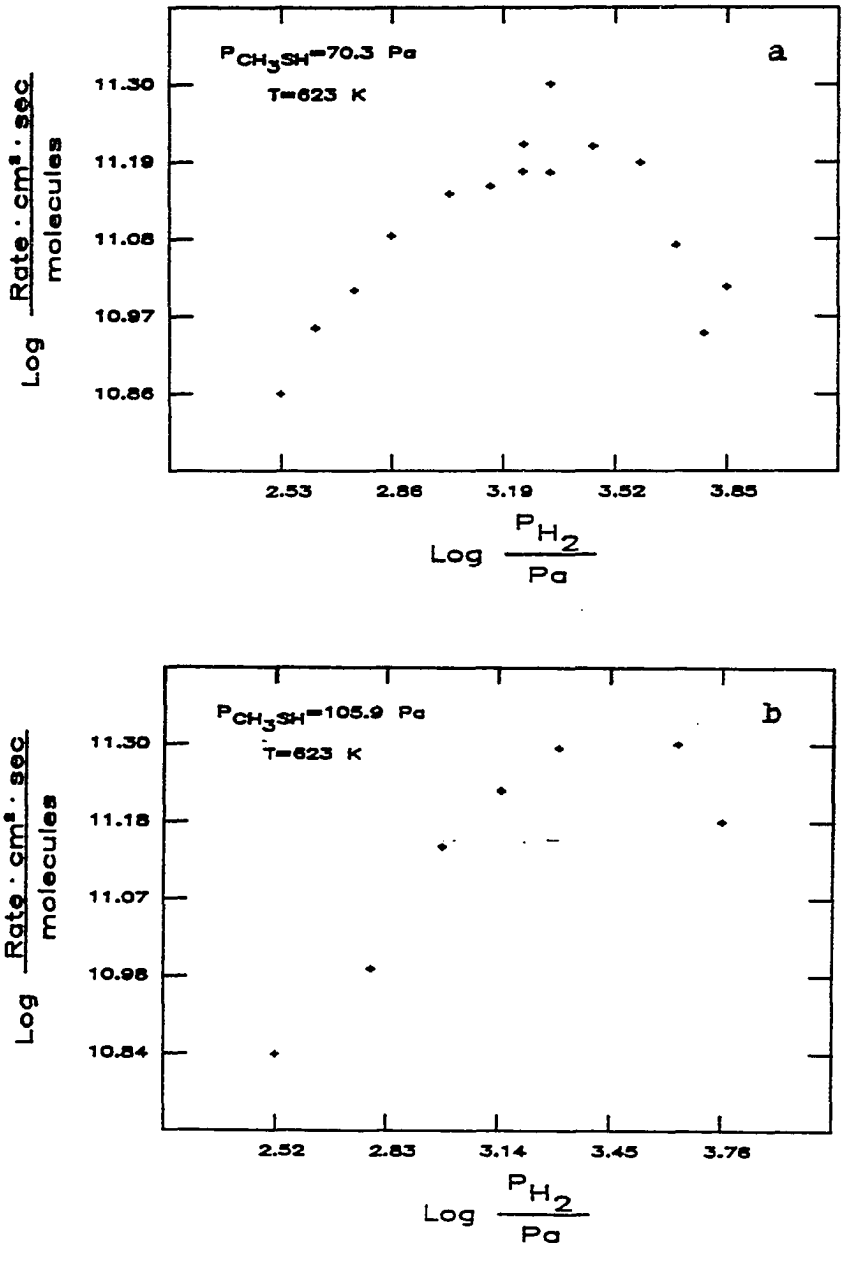

Figure I-6. Hydrogen order plots (623 K) at constant methanethiol pressures of 70.3 Pa (a) and 105.9 Pa (b)

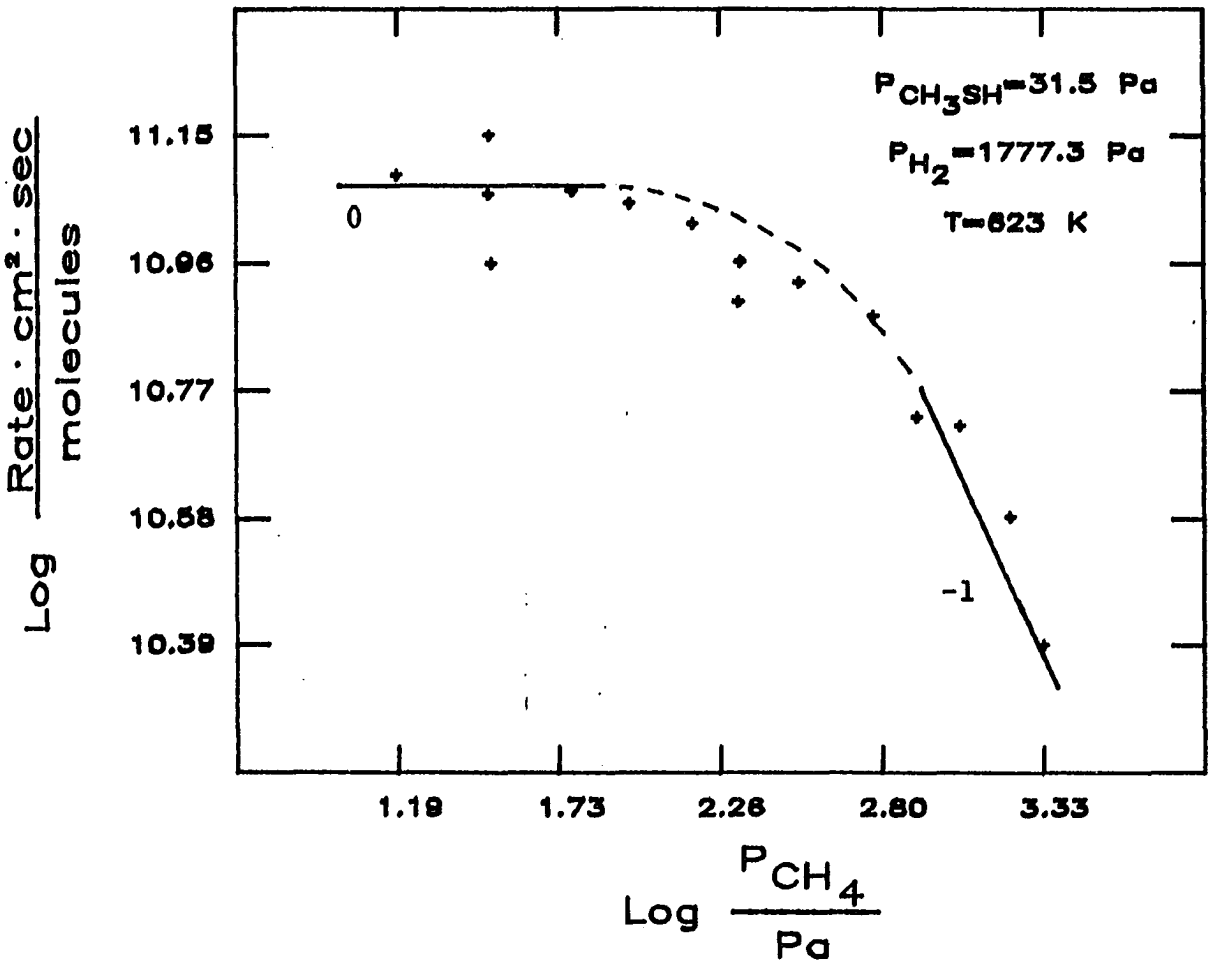

Figure I-7. Methane order plot (623 K) at a constant methanethiol pressure of 31.5 Pa and constant hydrogen pressure of 1777.3 Pa. The solid lines represent possible limiting pressure order dependencies

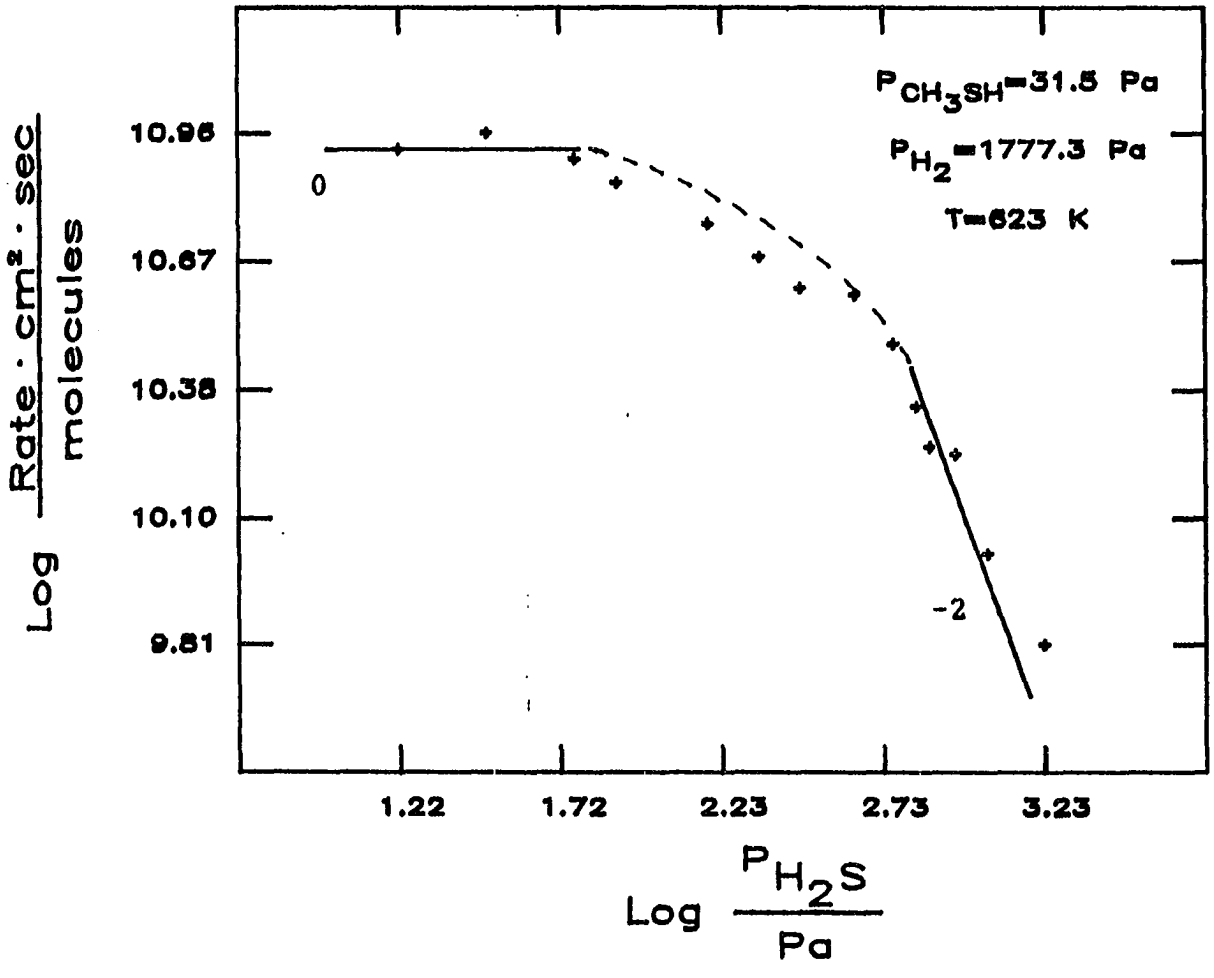

Figure I-8. Hydrogen sulfide order plot (623 K) at a constant methanethiol pressure of 31.5 Pa and constant hydrogen pressure of 1777.3 Pa. The solid lines represent possible limiting pressure order dependencies

expression was developed for the HDS of thiophenic compounds and not alkanethiols, it does provide a convenient starting point and is reproduced below. Recall that the denominator

$$\text{rate} = k \cdot \frac{K_S P_S}{(1+K_S P_S+\Sigma K_i P_i)^n} \cdot \frac{K_H P_H^m}{[1+K_H P_H^m]^p} \qquad \text{(I-1)}$$

in parentheses refers to the organosulfur adsorption site (an anion vacancy), while the denominator in brackets corresponds to the hydrogen adsorption site (a sulfur anion). These denominators will be referred to as the vacancy (or methanethiol) and sulfhydril denominators respectively. The individual pressure terms in these denominators represent the dominant adsorbate species on the surface. The numerator term represents the product of the pressure dependencies of the adsorbate species involved in the rate limiting step. These species need not be the dominant surface species (79). The generalized rate expression is based on a Langmuir-Hinshelwood kinetic formalism, which is described in Appendix I. This formalism is used in all mechanisms discussed below and it is assumed that the total number of active sites is independent of the reaction conditions and determined solely by the preparation and pretreatment of the catalyst.

Equation I-12 is this generalized rate expression with the exponents n, m, and p assigned values of 2, 1/2, and 1 respectively, with the constants combined, and where P_{SH} and

$$\text{rate} = \frac{aP_{SH}P_{H2}^{1/2}}{(1+bP_{SH})^2[1+cP_{H2}^{1/2}]} \qquad \text{(I-12)}$$

P_{H2} are the partial pressures of methanethiol and hydrogen respectively. These exponent assignments have been constrained to within the ranges found in the literature and are obviously inadequate when describing methanethiol HDS. The product inhibition terms have not been included in this expression and will be discussed later.

An obvious deficiency in this expression is its inability to generate the negative hydrogen order dependency. This may be accomplished in one of two ways:

1) Addition of a higher order hydrogen term, P_{H_2}, to the sulfhydril denominator. This term would represent a sulfur anion bonded to two hydrogen atoms.

2) Addition of a hydrogen term to the vacancy denominator. This term would represent hydrogen bonded directly to the tungsten.

The first possibility is unlikely since SH_2 type vibrations are not observed when WS_2 is saturated with either hydrogen or hydrogen sulfide (68). While direct evidence for the formation of a W-H species is lacking, the indirect evidence

described earlier suggests that, in addition to forming sulfur-hydrogen bonds, hydrogen competes with methanethiol for adsorption at these sulfur vacancies. To estimate the pressure dependency of the hydrogen-metal adsorbate it is useful to have some type of model for both the adsorption process and the adsorption site. The structure of the catalyst will be reviewed first with the aim of better defining the adsorption site; this review will be followed by a discussion of the hydrogen adsorption process.

WS_2 crystallizes in a lamellar structure, which is illustrated in Figure I-9. The characteristic repeating unit consists of a W layer sandwiched between two close packed sulfur layers, with each W cation at the center of a trigonal prism of six sulfur anions. The trigonal-prismatic coordination of WS_2 is unfavored electrostatically relative to an octahedral configuration and implies a highly covalent type of bonding (80). Bulk WS_2 is formed when these S-W-S units are stacked on top of each other and held together by van der Waals forces.

A top view of a single layer, Figure I-9b, allows one to distinguish three types of sulfur ions; a basal plane sulfur, S_C, and two edge sulfurs, S_A and S_B. Kalechite (81) has observed that in the presence of hydrogen these edge sulfurs, which are coordinated to the fewest metal atoms,

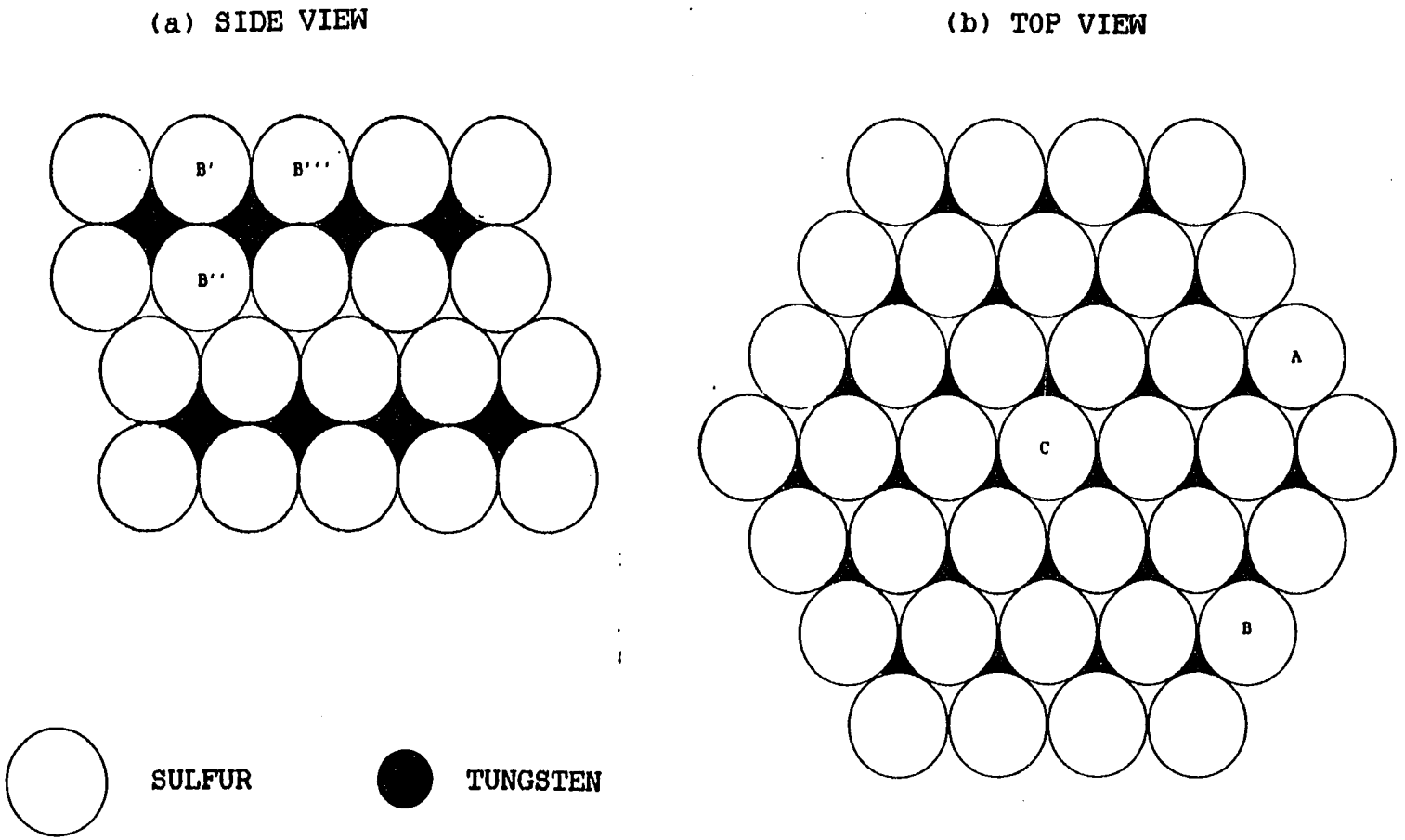

Figure I-9. Side (a) and Top (b) views of the structure of WS_2

are more easily removed than the basal plane sulfurs. It is these edge vacancies that are believed to be the sites of organosulfur adsorption. The two types of edge vacancies are defined by the number of "dangling metal bonds" exposed upon removal of the sulfur atom. Removal of an A sulfur exposes one "dangling bond" whereas a B sulfur vacancy exposes two "dangling bonds".

The number and arrangement of the vacancies during the course of the reaction is not well understood. Gachet et al. (53), using a $CoMo/Al_2O_3$ catalyst sulfided with a ^{35}S radioisotope, observed that a certain fraction of the catalyst's sulfur was labile in the sense that it could be displaced during the reaction with the sulfur of the organosulfur reactant. If this sulfur was removed by a high temperature hydrogen pretreatment it was replaced with reactant sulfur before any H_2S product was observed. Mirza et al. (52), in a similar series of experiments using ^{35}S labelled hydrogen sulfide, concluded that adsorbed sulfur was immobile. Together these observations suggest an immobile arrangement of sulfur (and vacancies) in a constant state of change resulting from the adsorption and desorption of sulfur.

When dealing with adsorption at a vacancy, a reasonable assumption is that each edge W atom can bond to as many

adsorbates as there are "dangling bonds". For example, a type A vacancy with one "dangling bond" can bond to either one sulfur or one hydrogen atom. A type B vacancy can bond to two hydrogen atoms but, due to size limitations, to only one sulfur atom.

Two hydrogen adsorption schemes that include hydrogen bonding at a vacancy were described earlier. The model proposed by Schuit (20) assumes a heterolytic dissociation of hydrogen in the initial adsorption step. A second sulfhyril group is formed in a subsequent step. Regardless of whether this adsorption occurs at a A or B type vacancy, the kinetic order in hydrogen pressure at low hydrogen pressures will be one-half.

The model of Fraser et al. (73) differs in that in the initial adsorption step hydrogen does not dissociate heterolytically but bonds only to the exposed metal. For an A type site this may occur via the dissociative adsorption of hydrogen on two A vacancies and, as in the previous scheme, will lead to a half order hydrogen dependence at low hydrogen pressures. A first order dependence is generated if the adsorption occurs at a single B type vacancy, which has two "dangling bonds" with which to interact with two hydrogen atoms.

In order to generate the sharp peak observed in the hydrogen order plots a hydrogen adsorbate with a first order dependence is necessary in the organosulfur denominator of equation I-12; hence the methanethiol adsorption site is defined as a B type vacancy. The hydrogen adsorption model of Fraser et al., adapted for a B type site, is shown in equations I-13 through I-15. S represents a sulfur atom

$$H_2 + *_b \text{ <===> } H_2*_b \qquad \text{(I-13)}$$

$$H_2*_b + S \text{ <===> } H*_b + HS \qquad \text{(I-14)}$$

$$H*_b + S \text{ <===> } *_b + HS \qquad \text{(I-15)}$$

adjacent to a B type vacancy and $*_b$ represents the B type vacancy. This mechanism is very similar to the heterolytic adsorption scheme of Schuit except that adsorbed hydrogen species is stabilized by the second W orbital prior to undergoing the severe polarization necessary in a single step heterolytic bond cleavage.

The pressure dependencies corresponding to this hydrogen adsorption sequence are

$$[H_2*_b] = K_{13}P_{H2}[*_b] \qquad \text{(I-13a)}$$

$$[H*_b] = (K_{13}K_{14}/K_{15})^{1/2}P_{H2}^{1/2}[*_b] \qquad \text{(I-14a)}$$

$$[HS] = (K_{13}K_{14}K_{15})^{1/2}\ P_{H2}^{1/2}[S] \qquad \text{(I-15a)}$$

A second modification of equation I-12 pertains to the methanethiol adsorption term in the vacancy denominator. The generalized rate expression was developed for thiophenic-type compounds which adsorb molecularly, whereas methanethiol adsorbs dissociatively (77,78). This most likely occurs in a manner similar to the dissociative adsorption of H_2S (68):

$$CH_3SH + *_b + S \langle===\rangle CH_3S*_b + HS \qquad (I\text{-}16)$$

$$[CH_3S*_b] = \frac{K_{16}P_{SH}[S][*]}{[HS]} \qquad (I\text{-}16a)$$

Adsorption at a B type vacancy implies a bridged thiomethoxy species. Such species are more common in transition-metal complexes than the terminally bound thiomethoxy groups (82). The methyl group in bridging dimolybdenum complexes (83,84) forms an angle of ~115 degrees with the Mo-S-Mo plane. For steric reasons, a slightly larger angle is necessary when methanethiol adsorbs at a B type vacancy with the methyl group oriented toward the adjacent sulfur atoms.

The sulfhydril terms in equation I-16a, [S] and [HS], can be eliminated using the hydrogen adsorption sequence described previously. Combining these two adsorption processes yields equation I-16b for the pressure dependency

$$[CH_3S*_b] = \frac{K_{16}P_{SH}[*]}{(K_{13}K_{14}K_{15})^{1/2}P_{H2}^{1/2}} \qquad \text{(I-16b)}$$

of dissociative methanethiol adsorption. Thus, the organosulfur term must be changed from P_{SH} to $P_{SH}/P_{H2}^{1/2}$.

Using the modifications suggested by the methanethiol and hydrogen adsorption sequences, equation I-12 becomes

$$\text{rate} = \frac{aP_{SH}P_{H2}^{1/2}}{\left(1+bP_{H2}+c\frac{P_{SH}}{P_{H2}^{1/2}}\right)^2} \cdot \frac{1}{\left[1+dP_{H2}^{1/2}\right]} \qquad \text{(I-17)}$$

The $P_{H2}^{1/2}$ term corresponding to the $H*_b$ species has not been included in this equation. "Best fits" were attained without including fractional hydrogen dependencies of this type and so for convenience it was not included. The absence of such a term implies that the equilibrium of the first migratory step (equation I-14) lies far to the left and/or the equilibrium of the second migratory step (equation I-15) lies far to the right.

A reaction sequence using the proposed hydrogen and methanethiol adsorption steps just described is shown in equations I-18 through I-23 and will be referred to as the

$$H_2 + *_b \langle===\rangle H_2*_b \qquad \text{(I-18)}$$

$$H_2*_b + S \langle===\rangle H*_b + HS \qquad \text{(I-19)}$$

$$H^{*}_{b} + S \langle ===\rangle {}^{*}_{b} + HS \qquad \text{(I-20)}$$

$$CH_3SH + {}^{*}_{b} + S \langle ===\rangle CH_3S^{*}_{b} + HS \qquad \text{(I-21)}$$

$$CH_3S^{*}_{b} + {}^{*}_{b}H + HS \text{ ---}\rangle CH_4 + HS^{*}_{b} + S + {}^{*}_{b} \qquad \text{(I-22)}$$

$$HS^{*}_{b} + HS \text{ ---}\rangle H_2S + {}^{*}_{b} + S \qquad \text{(I-23)}$$

single vacancy formulation or mechanism. The mathematical development leading to the rate expression is shown in Appendix II, and assumes the establishment of equilibrium in those steps preceding the rate limiting step, equation I-22. The sulfhydril species is included in this step to account for Maternova's observation (70) that the rate is proportional to the concentration of sulfhydril hydrogen. The involvement of two vacancy sites is necessary to generate the negative orders in hydrogen and methanethiol. Likewise, the proposed species occupying these vacancies in the rate limiting step are necessary to generate the observed positive order dependencies.

Conceptually, the rate limiting step involves the simultaneous interaction of the vacancy and sulfhydril hydrogens with the thiomethoxy group, CH_3S. It was mentioned earlier that SH_2 type vibrations are not observed when WS_2 is saturated with either hydrogen or hydrogen sulfide (67). This suggests that adsorbed sulfur bonds to

only one substituent other than tungsten and that the interaction of the vacancy hydrogen with the thiomethoxy sulfur weakens the carbon-sulfur bond. When this bond weakening occurs simultaneously with the hydrogen-methyl interaction, HS^*_b and methane are formed.

The formation of hydrogen sulfide occurs in the final step of the mechanism. If the concentration of the HS^*_b species is assumed small (an assumption supported by the fact that inclusion of the term corresponding to this species in the rate expression does not improve the fit), then this mechanism generates a rate expression identical to equation I-17. The calculated curves for the single vacancy mechanism and rate expression, the dotted lines in Figures I-10 through I-13, have the general shapes of the data and the fits are rather good for such a simple equation. The values for the parameters in equation I-17 are shown in Table I-1. The calculated curves underestimate the rate in the low pressure hydrogen range in Figure I-10 and are insufficiently flat in the center of the methanethiol plot shown in Figure I-12. Improvements can only result from changing the rate expression and the mechanism from which it was derived. This will undoubtedly involve an increase in the number of parameters used to fit the data and this number will be kept as small as possible. Two possible

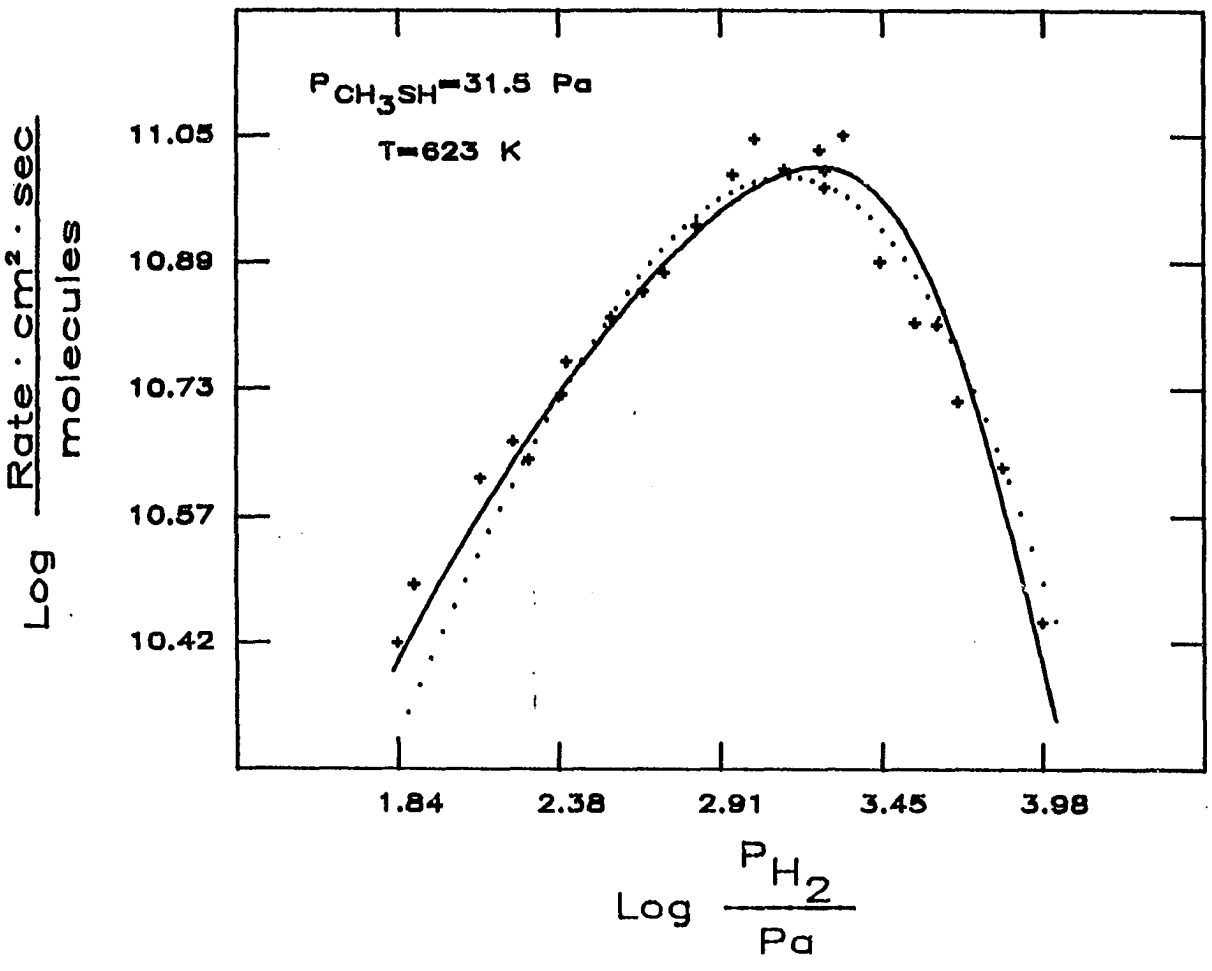

Figure I-10. Calculated fit of the hydrogen order plot (methanethiol pressure of 31.5 Pa). The parameter values used in the single vacancy (·····) and paired vacancies (———) rate expressions are listed in Table I-1

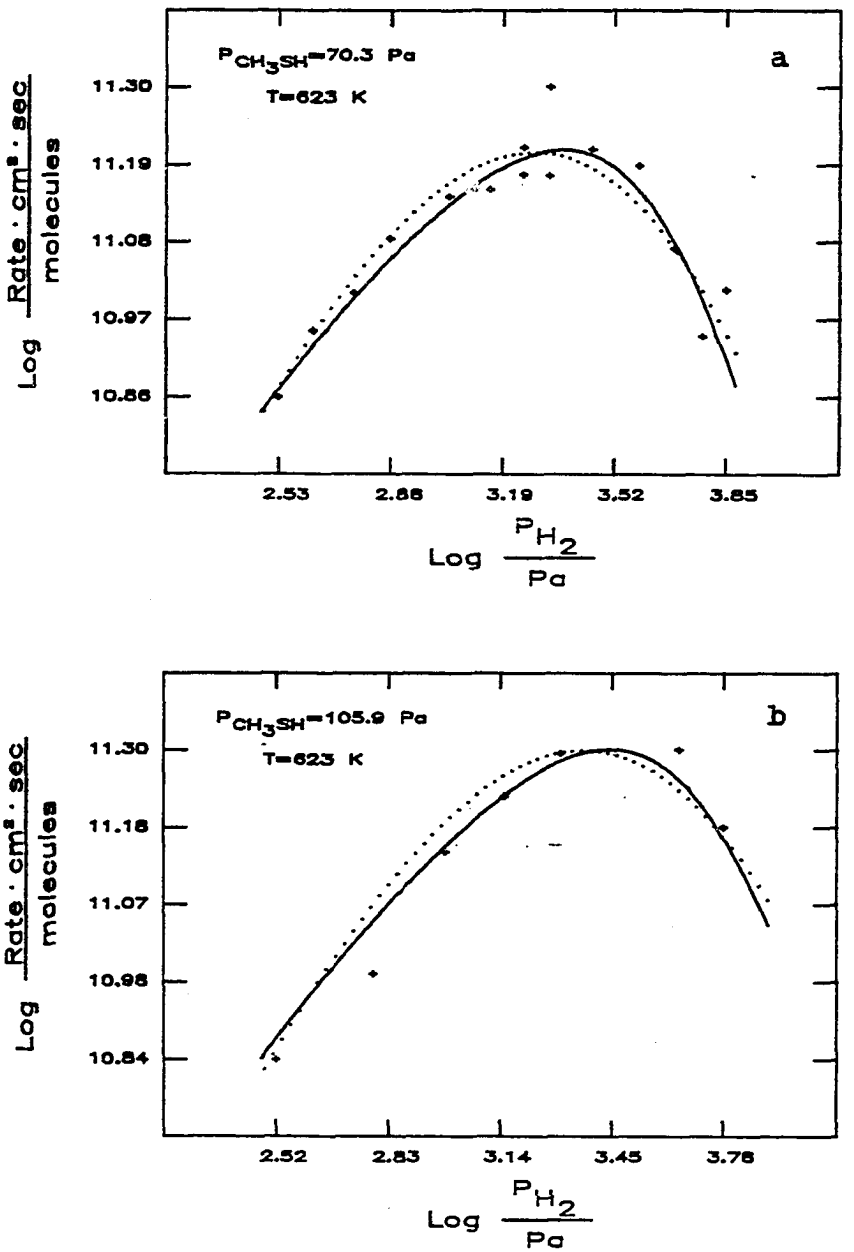

Figure I-11. Calculated fits of the hydrogen order plots (methanethiol pressures of 70.3 Pa (a) and 105.9 Pa (b)). The parameter values used in the single vacancy (•••••) and paired vacancies (———) rate expressions are listed in Table I-1

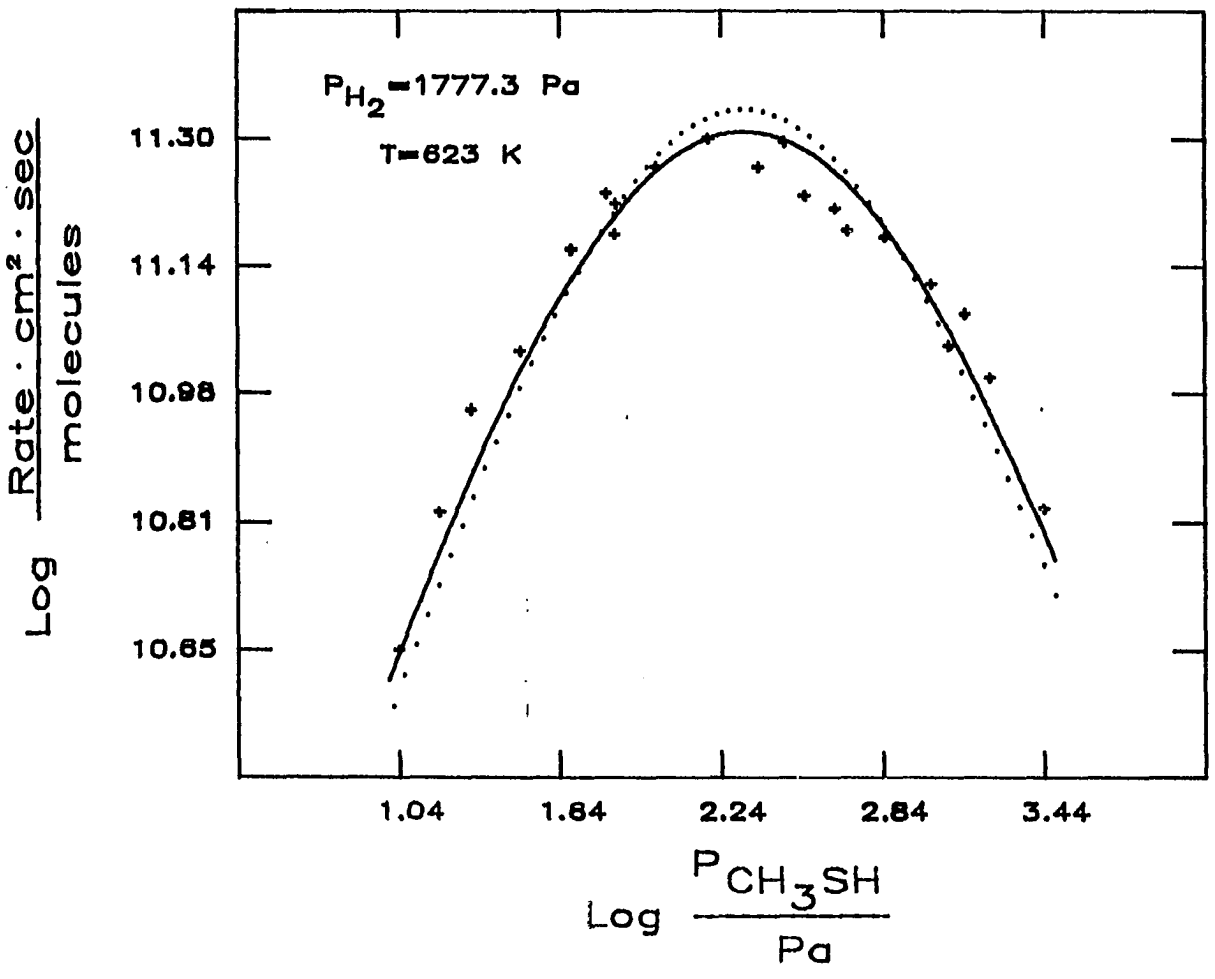

Figure I-12. Calculated fit of the methanethiol order plot (hydrogen pressure of 1777.3 Pa). The parameter values used in the single vacancy (·····) and paired vacancies (———) rate expressions are listed in Table I-1

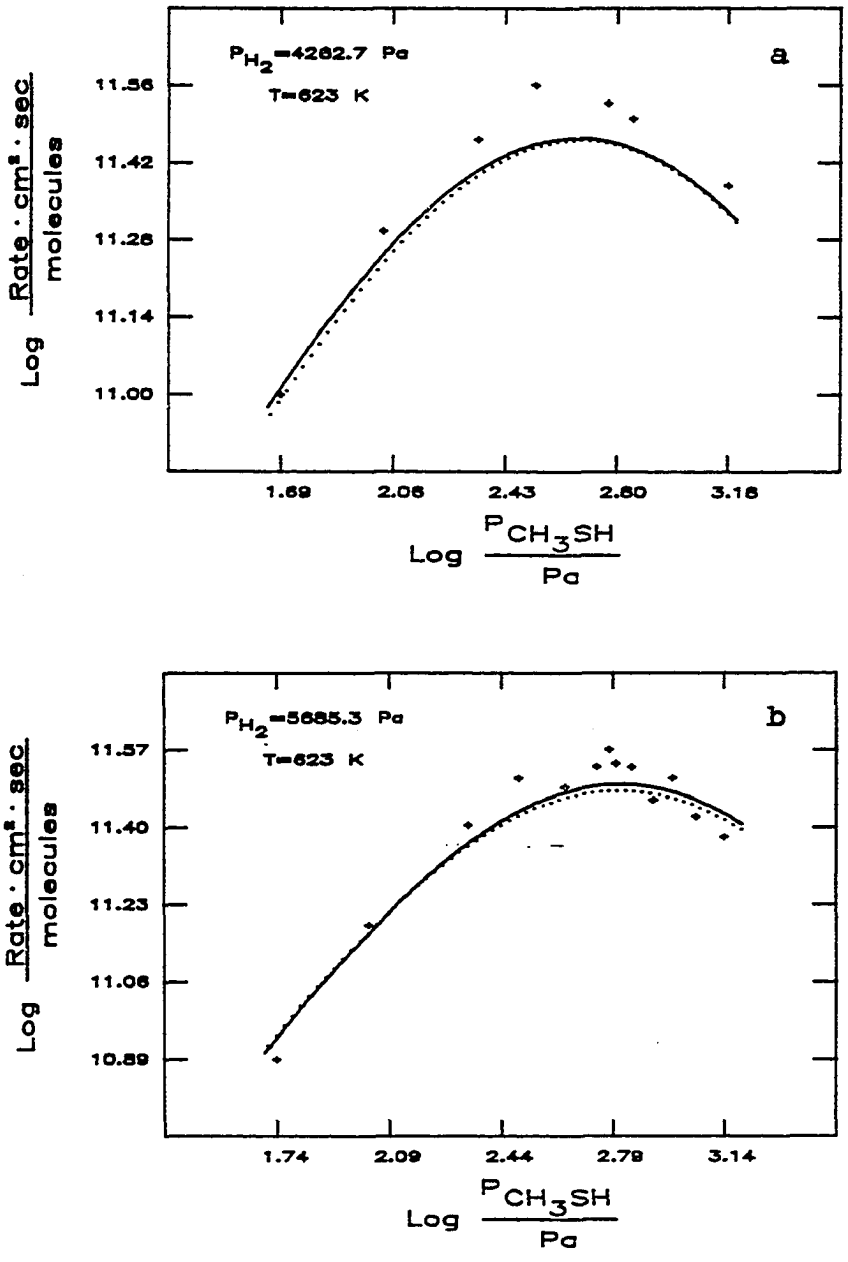

Figure I-13. Calculated fits of the methanethiol order plots (hydrogen pressures of 4262.7 Pa (a) and 5685.3 Pa (b)). The parameter values used in the single vacancy (·····) and paired vacancies (———) rate expressions are listed in Table I-1

Table I-1. Parameter values used to fit the experimental data

Parameter	Single Vacancy Formalism[a] (Equation I-17) Value	Units	Paired Vacancies Formalism[b,c] (Equations I-36 and I-42) Value	Units
a	3.935×10^{8}	$\frac{\text{molecules}}{Pa^{3/2} \cdot cm^2 \cdot sec}$	8.263×10^{8}	$\frac{\text{molecules}}{Pa^{3/2} \cdot cm^2 \cdot sec}$
b	2.436×10^{-4}	Pa^{-1}	0.0	---
c	0.283	Pa^{-1}	7.65×10^{-8}	Pa^{-2}
d	0.0235	$Pa^{-1/2}$	0.728	$Pa^{-1/2}$
e	---	---	0.0	---
f	---	---	0.0478	Pa^{-1}
g	---	---	0.118	$Pa^{-1/2}$
h	---	---	1.95×10^{-3}	Pa^{-1}
i	---	---	0.323	$Pa^{-1/2}$
j	---	---	7.358×10^{-3}	Pa^{-1}

[a] RMSD (root mean squared percent deviation) = 11.89 (reactant data only).

[b] RMSD (root mean squared percent deviation) = 9.91 (reactant data only).

[c] Equation I-36 does not include parameters h, i and j; Equation I-42 does not include parameters b and e.

rationales for such a modification are found in the literature. The first to be discussed, the paired vacancies formulation or mechanism, assumes that the vacancies exist in pairs and that the organosulfur adsorption site is defined as two adjacent vacancies. The second proposal, the two site formulation or mechanism, assumes that the HDS reaction takes place at two independent active centers. The essence of the previous mechanism is retained in both of the new mechanisms.

The paired vacancies formulation is based on the work of Tanaka and Okuhara (78), who have defined the active center for hydrogenation, isomerization and exchange reactions on Ni_2S_3 and MoS_2 in terms of two or three vacancies (two or three"dangling bonds") associated with a single metal atom. This type of active center description was originally proposed by Siegal (85) for oxide catalysts and adsorption at these sites is descriptively similar to ligand bonding in homogeneous catalysts. Two adjacent B type vacancies (four "dangling bonds") will define the methanethiol adsorption site in the mechanism described below, The same number and type of vacancies were involved in the rate limiting step of the previous mechanism. Supportive evidence for the existence of paired vacancies is limited and based on O_2 and NO adsorption studies (61). The dissociative adsorption of

oxygen requires two vacancies and since NO adsorbs as a dimer with twice the stoichiometry of O_2 adsorption, this necessitates that these vacancies be adjacent. Recall that linear relationships between O_2 and NO uptake and HDS activity have been observed (57-60). If the methyl group of the CH_3S moiety does not diffuse across the sulfur anions, then the formation of methyl sulfide (at high methanethiol/hydrogen ratios) seen in this study and by Wilson and Kemball (77) requires two methanethiol molecules to adsorb on adjacent sites since adsorbed sulfur does not diffuse between vacancies (52).

It is to be expected that the number of adsorption steps will be larger using this formalism since, for example, adsorption of a single methanethiol now occupies only half the adsorption site whereas in the previous mechanism it completely occupied the site. The reaction sequence for this formalism is shown in equations I-24 through I-35. The

$$H_2 + *_b \text{ <===> } H_2*_b \qquad \text{(I-24)}$$

$$H_2 + H_2*_b \text{ <===> } H_2*_bH_2 \qquad \text{(I-25)}$$

$$H_2*_b + S \text{ <===> } H*_b + HS \qquad \text{(I-26)}$$

$$H*_b + S \text{ <===> } *_b + HS \qquad \text{(I-27)}$$

$$H_2*_bH_2 + S \text{ <===> } H_2*_bH + HS \qquad \text{(I-28)}$$

$$H_2{*_b}H + S \langle===\rangle H_2{*_b} + HS \quad \text{(I-29)}$$

$$CH_3SH + {*_b} + S \langle===\rangle CH_3S{*_b} + HS \quad \text{(I-30)}$$

$$CH_3SH + {*_b}H + S \langle===\rangle CH_3S{*_b}H + HS \quad \text{(I-31)}$$

$$CH_3SH + H_2{*_b} + S \langle===\rangle CH_3S{*_b}H_2 + HS \quad \text{(I-32)}$$

$$CH_3SH + CH_3S{*_b} + S \langle===\rangle CH_3S{*_b}SCH_3 + HS \quad \text{(I-33)}$$

$$CH_3S{*_b}H + HS \longrightarrow CH_4 + HS{*_b} + S \quad \text{(I-34)}$$

$$HS{*_b} + HS \longrightarrow H_2S + {*_b} + S \quad \text{(I-35)}$$

most obvious effect of the redefinition is the larger number of steps and surface intermediates. Equations I-24, I-26, I-31, I-34 and I-35 are the steps leading to product formation and are similar to those of the single vacancy mechanism. As before, the rate limiting step (equation I-34) involves the breaking of the carbon-sulfur bond and formation of methane. Hydrogen sulfide is formed in the last step and the concentration of the $HS{*_b}$ species will be assumed small (an assumption supported by the fact that inclusion of the term corresponding to this species in the rate expression does not improve the fit).

Several of the intermediates; $CH_3S{*_b}H_2$, $CH_3{*_b}H$ and $H_2{*_b}H$, can be formed using different adsorption sequences. Since the pressure dependencies are the same regardless of

the sequence, only a single sequence has been presented for each of these intermediates.

The number of surface intermediates could be reduced if the surface concentration of the H^*_b type species is assumed to be small. This is true if the equilibria of the initial migratory steps (equations I-26 and I-28) lie far to the left or if the equilibria of the second migratory steps (equations I-27 and I-29) lie far to the right. (A similar assumption was used in the single vacancy formulation.) This assumption implies that the concentrations of those intermediates dependent on this hydrogen adsorption sequence; $^*_bH$, $H_2{}^*_bH$, and $CH_3S^*_bH$, will be small relative to the concentrations of the other surface intermediates. The inclusion of terms corresponding to these species in the rate expression does not lead to an improvement of fit.

This new mechanism and its restrictions generate the rate expression shown in equation I-36. The mathematical

$$\text{rate} = \frac{aP_{SH}P_{H_2}^{1/2}}{\left(1+bP_{H_2}+cP_{H_2}^2+d\frac{P_{SH}}{P_{H_2}^{1/2}}+eP_{SH}P_{H_2}^{1/2}+f\frac{P_{SH}^2}{P_{H_2}}\right)} \cdot \frac{1}{\left[1+gP_{H_2}^{1/2}\right]} \qquad \text{(I-36)}$$

development resulting in equation I-36 is shown is Appendix III. The P_{H_2} and $P_{H_2}^2$ terms in the denominator represent adsorbed hydrogen occupying half and all of the "dangling

bonds" of the two adjacent B type vacancies. Likewise, $P_{SH}/P_{H_2}^{1/2}$ and P_{SH}^2/P_{H_2} represent adsorbed methanethiol that half fills and completely fills the two vacancy site. The $P_{SH}P_{H_2}^{1/2}$ term represent the "mixed" adsorbate, $CH_3S*_bH_2$, where methanethiol fills one vacancy and dihydrogen the other.

The calculated curves for the paired vacancies formulation are also shown in Figures I-10 through I-13. Five parameters are required for this fit (see Table I-1), one more than for the single vacancy formulation. The hydrogen order curves undergo a slight shift in the maximum to higher hydrogen pressures and exhibit an improved fit prior to the peak maximum. This improvement is most easily seen at the low hydrogen pressure region in Figure I-10. A more modest improvement is seen in the methanethiol order plots; primarily a small broadening of the curve in Figure I-12.

Both the visual comparison of the two calculated curves and a comparison the corresponding RMSDs in Table I-1 (a 17% improvement) suggests that the improved fit of the paired vacancies mechanism is sufficient to warrant its selection over the single vacancy mechanism. Wright et al. (68) observed that hydrogen saturation of WS_2 occurred at ~500 Torr and if the number of sulfhydril sites is assumed to be large relative to the number of vacancy sites then the

sulfhydril parameters (d and f for the single and paired vacancies formulations respectively) can also be used as a selection criterion. The paired vacancies value yields 97% saturation at 500 Torr whereas 86% saturation coverage is calculated for the single vacancy formulation. The paired vacancies formulation therefore also provides a better interpretation of the hydrogen saturation result.

The single vacancy site mechanism assumes that adjacent B type vacancies are independent whereas the paired vacancies site mechanism infers a chemical interrelationship between these vacancies. This interrelationship would exist if the vacancies occurred on the same tungsten atom, as proposed by Valyon and Hall (61). Figure I-9b shows that adjacent B type vacancies share at least one tungsten atom. Two possible geometries exist for these paired vacancies: (1) pairing in the basal plane (the vacancies are formed by the removal of sulfurs B' and B''), and (2) pairing in the c-axis direction (vacancies are formed by the removal of sulfurs B' and B''). The pairing in the c-axis direction is more reasonable since it allows the vacancy hydrogen and the sulfur lone pair in the thiomethoxy group to interact in the rate limiting step (of either mechanism) whereas a similar geometry is not present in the basal plane vacancy arrangement. The c-axis pairing arrangement is identical to

the promoter stabilized active site geometry proposed by Farragher and Cossee in their edge intercalation model (19).

The additional adsorbate term in the paired vacancies formulation, $P_{SH}/P_{H2}^{1/2}$, corresponds to a single methanethiol molecule occupying one of the two vacancies. Pairing of the vacancies parallel to the c-axis suggests that when the methyl group of the adsorbed methanethiol is oriented toward the adjacent vacancy it sterically hinders further adsorption at this site. Inversion of the methyl group about the sulfur then exposes the adjacent vacancy to adsorption.

The paired vacancies fit can be improved by including a P_{H2} term in the vacancy denominator ($b \neq 0$). Such a term could represent dihydrogen adsorbed at one of the B type vacancies in a manner similar to that in the last mechanism. This adsorbate is the precursor to sulfhydril formation and complete filling of the adsorption site by two dihydrogen molecules (P_{H2}^2 pressure dependence). The term could also represent two bridging hydrogens (one at each vacancy) that effectively block the site to further adsorption. The effect of this term on the calculated curves is to diminish, somewhat, the change resulting from the $P_{SH}/P_{H2}^{1/2}$ term. Since the improvement is rather small (a decrease in the RMSD of less than 5%) this term was not included and the fits are not presented.

Poisoning studies, which show a leveling off of activity with increasing poison concentration and not an extrapolation to zero activity, suggest the existence of two independent active sites. The addition of a second independent site to the mechanism generates a rate equation that is the sum of two polynomial expressions. Such an expression can generate a curve with two peaks or one broad peak, as is seen for the methanethiol order plot shown in Figure I-5. The possibility of two independent sites was investigated assuming that the two sites consisted of paired A and B type vacancies with mechanisms similar to that just described for paired B type sites. As expected, the rate expression using the minimum number of parameters (7) did fit the above mentioned methanethiol curve, Figure I-5, quite well (i.e., a very flat peak). However the overall fit (a RMSD of 9.70) was only marginally better than the 5 parameter paired vacancies fit (a RMSD of 9.91). The best fit attained using this formulation (also the best fit out of all three formulations) required nine parameters. It was felt that the degree of improvement did not justify the added complexity of the rate expression and mechanism, so the two site mechanism is not presented in detail. The sulfhydril coverage calculated from this model, using parameters giving best fits to the kinetic data, was

seriously underestimated (72%) for a hydrogen pressure of 500 Torr.

The discussion so far has not dealt with the product gas inhibition results and these results will be discussed using the paired vacancies formalism. Hydrogen sulfide adsorbs dissociatively with the abstracted hydrogen forming a sulfhydril bond (68). This is the reverse of the H_2S formation step, equation I-35, and is similar to the adsorption of methanethiol. At high pressures, H_2S may be expected to completely fill the vacancy site, thus generating a species having the observed second order hydrogen sulfide dependence. The H_2S adsorption sequence is

$$H_2S + *_b + S \text{ <===> } HS*_b + HS \qquad \text{(I-37)}$$

$$H_2S + HS*_b + S \text{ <===> } HS*_bSH + HS \qquad \text{(I-38)}$$

This adsorption processes implies a $P_{H2S}/P_{H2}^{1/2}$ dependence for the HS* species and a P_{H2S}^2/P_{H2} dependence for the $HS*_bSH$ species.

The proposed scheme of methane adsorption, unlike that of H_2S, does not resemble the reverse of its formation step, equation I-34. Exchange of methane and deuterium (P_{CH4}=710 Pa and P_{D2}=1777 Pa, 623 K) was not observed under conditions where methane inhibits the reaction. Wilson and Kemball (77) have estimated that the exchange of methanethiol and

deuterium occurs at ~ 1/100 the rate of methane formation in the HDS of methanethiol over WS_2 (P_{CH_3H}=2.7 x 10^3 Pa and P_{H_2}=2.8 x 10^4 Pa, 593 K). These results suggest that the dissociative adsorption of methane does not involve bonding to sulfur, since such a scheme would most likely lead to deuterated methane. In an adsorption scheme that avoids this problem, equation I-39, methane adsorbs dissociatively

$$CH_4 + *_b \text{ <===> } H*_bCH_3 \qquad \text{(I-39)}$$

at a paired vacancies site with both fragments bonding to the exposed tungsten. Adsorption in this manner generates a P_{CH_4} pressure dependency for the CH_3*H species.

The possibilty of forming "mixed adsorbates" also exists for methane and hydrogen sulfide adsorption. For methane, the only possibility is adsorption at a $*_bH$ site. For hydrogen sulfide, the possibilities are more numerous and adsorption can occur at the $*_bH$, $*_bH_2$ and $*_bSCH_3$ half-filled sites. While it may be possible to reasonably dismiss some of these intermediates, the data are insufficient to clearly distinguish among all of them. (To make such an elimination would require additional inhibition curves at different reactant pressures.) Since a determination of the proper pressure dependencies for the inhibition terms cannot be made, it will be assumed that product adsorption and inhibition occur in the manner described above.

The above adsorption steps generate equation I-40 for methane inhibition and equation I-41 for hydrogen sulfide inhibition. The values of the constants in these expres-

$$\text{rate} = \frac{1.837 \times 10^{11}}{\left(1.813 + hP_{CH_4}\right)} \qquad \text{(I-40)}$$

$$\text{rate} = \frac{1.837 \times 10^{11}}{\left(1.813 + i\frac{P_{H_2S}}{P_{H_2}^{1/2}} + j\frac{P_{H_2S}^2}{P_{H_2}}\right)} \qquad \text{(I-41)}$$

sions were calculated using the best fit parameter values (paired vacancies rate expression, equation I-36) shown in Table I-1. The fits for methane and hydrogen sulfide inhibition are shown in Figures I-14 and I-15. The calculated methane curve, Figure I-14, has the shape of the data but underestimates the rate (~15%) at low methane pressures. The calculated hydrogen sulfide curve, Figure I-15, fits the data quite well in all regions.

Equation I-42 is a combination of the reactant and product rate expressions, and is shown below with the relationships between the non-zero parameters and the rate and equilibrium constants of the paired vacancies mechanism.

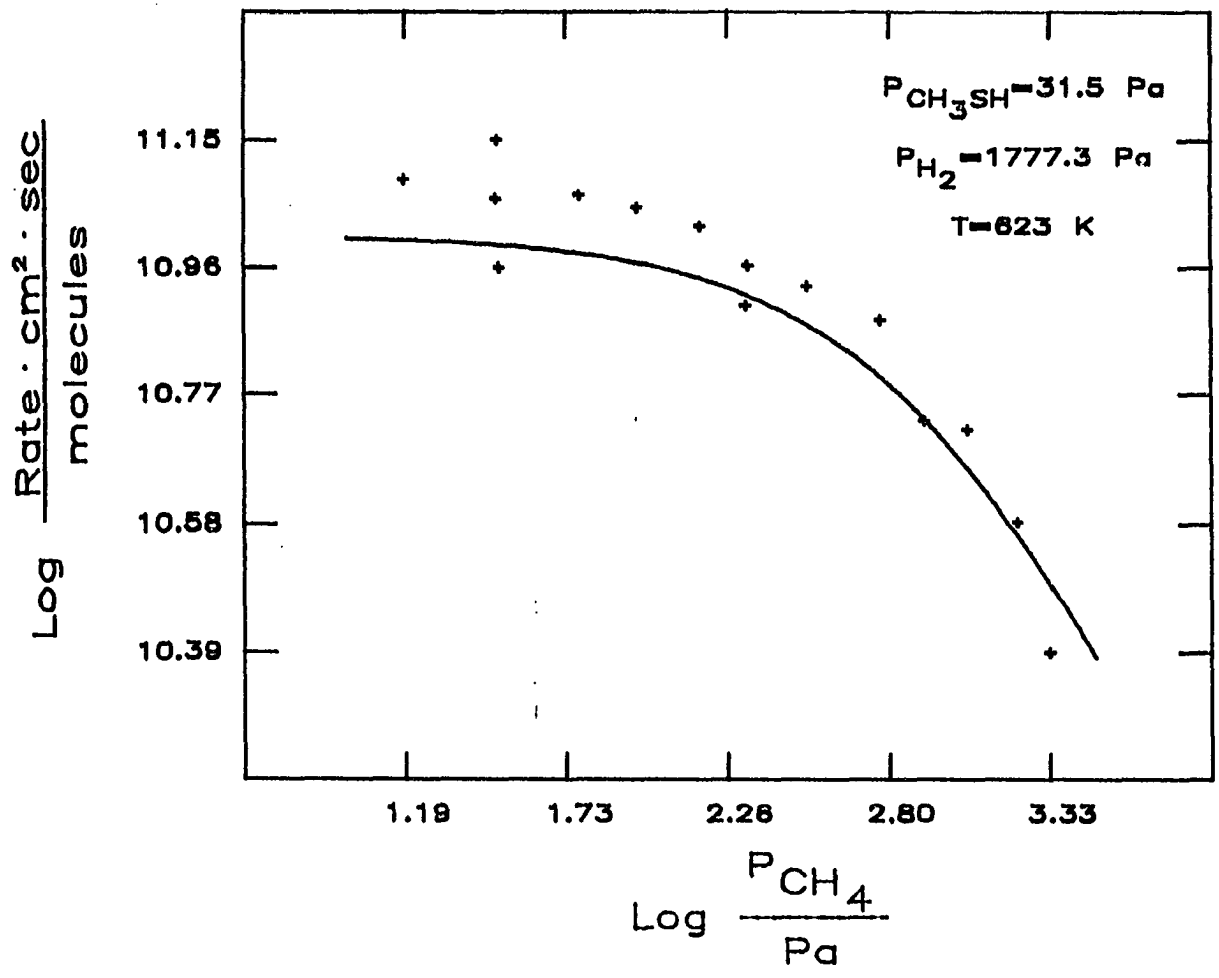

Figure I-14. Calculated fit of the methane order plot (methanethiol pressure of 31.5 Pa and hydrogen pressure of 1777.3 Pa). The parameter values used in the paired vacancies rate expression are listed in Table I-1

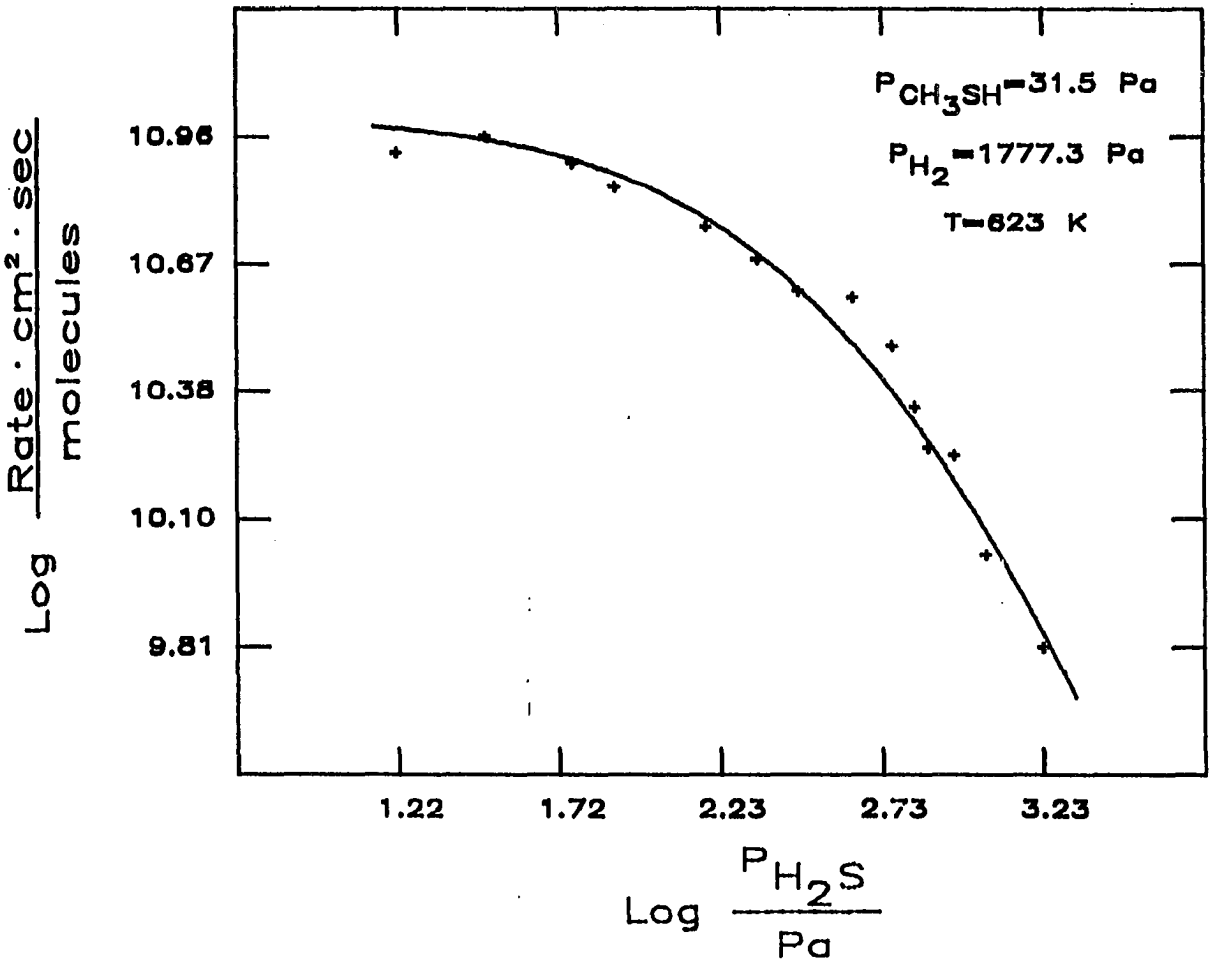

Figure I-15. Calculated fit of the hydrogen sulfide order plot (methanethiol pressure of 31.5 Pa and hydrogen pressure of 1777.3 Pa). The parameter values used in the paired vacancies rate expression are listed in Table I-1

$$\text{rate} = \frac{aP_{SH}P_{H_2}^{1/2}}{\left(1+cP_{H_2}^2+d\frac{P_{SH}}{P_{H_2}^{1/2}}+f\frac{P_{SH}^2}{P_{H_2}}+hP_{CH_4}+i\frac{P_{H_2S}}{P_{H_2}^{1/2}}+j\frac{P_{H_2S}^2}{P_{H_2}}\right)} \cdot \frac{1}{\left[1+gP_{H_2}^{1/2}\right]}$$

$$a = k_{34}K_{31}(K_{24}K_{26}/K_{27})^{1/2} \qquad g = (K_{24}K_{26}K_{27})^{1/2}$$

$$c = K_{24}K_{25} \qquad h = K_{39}$$

$$d = K_{30}/(K_{24}K_{26}K_{27})^{1/2} \qquad i = K_{37}/(K_{24}K_{26}K_{27})^{1/2}$$

$$f = K_{33}K_{30}/(K_{24}K_{26}K_{27}) \qquad j = K_{37}K_{38}/(K_{24}K_{26}K_{27})$$

(I-42)

It is apparent from this equation, and the accompanying parameter definitions, that the temperature dependence of the reaction rate is a composite value made up of contributions not only from the rate constant of the limiting step, but also the equilibrium constants of those steps prior to the rate limiting step (in the absence of product adsorption). The temperature dependence of the reaction rate at reactant pressures of 31.5 Pa (.236 Torr) CH_3SH and 1.777×10^3 Pa (13.33 Torr) H_2 is shown, in Arrhenius form, in Figure I-16. The apparent activation energy of 24.9 kJ/mole (5.9 kcal/mole) is, at first glance, surprisingly low, although as Table I-2 shows, it is within the observed range of values. This range of energies can be rationalized within the Langmuir-Hinshelwood kinetic

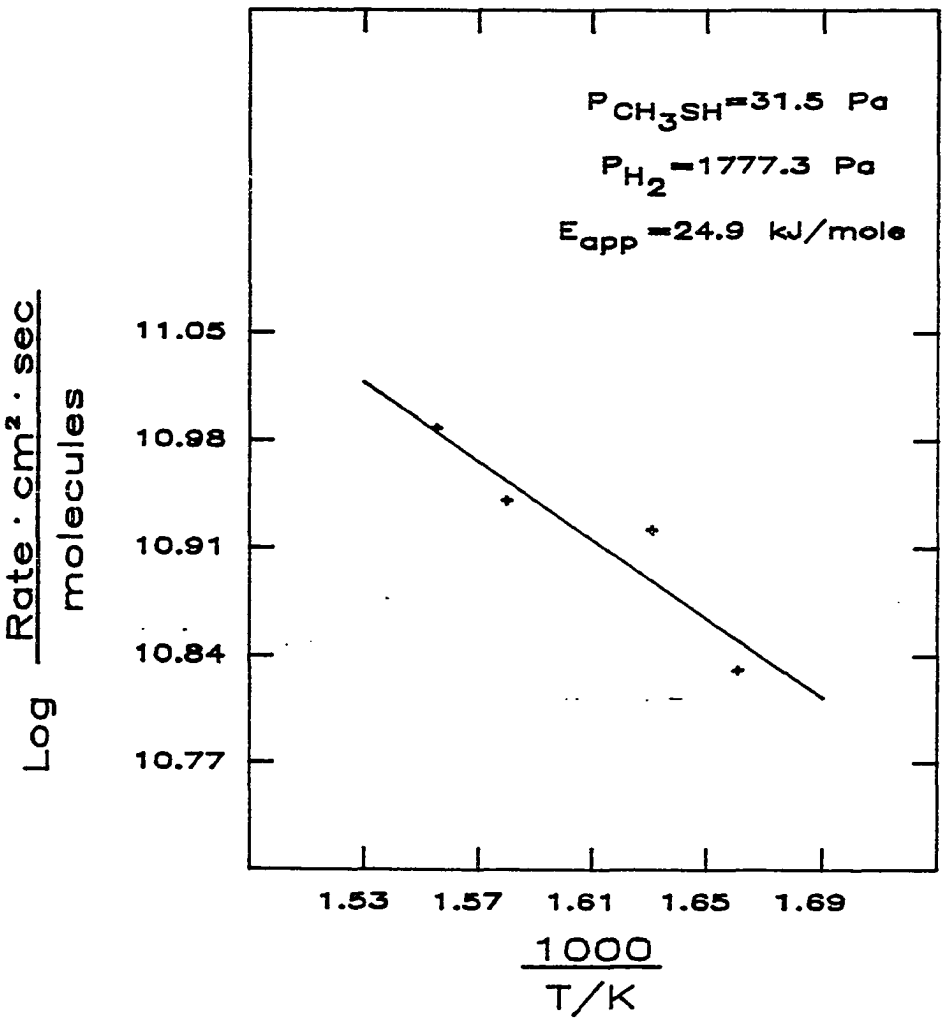

Figure I-16. Temperature dependence of the reaction at a constant methanethiol pressure of 31.5 Pa and constant hydrogen pressure of 1777.3 Pa

Table I-2. Apparent activation energy values of the HDS reaction

Catalyst	Organosulfur compound	Temperature Range (K)	P_{Total} (Atm)	$\frac{P_{H_2}}{P_{SH}}$	E_{app} $\left(\frac{kJ}{mole}\right)$	Ref.
$\frac{CoMo^a}{Al_2O_3}$	Thiophene	508-538	1		15.5	37
$\frac{CoMo}{Al_2O_3}$	Thiophene	523-543 573-623	1 1	77/1 77/1	84 40	87
$\frac{CoMo}{Al_2O_3}$	Thiophene	522-586	1		49.8	88
$\frac{NiMo}{Al_2O_3}$	Thiophene	510-563	1	300/1	12.6	89
WS_2	Thiophene	545-577	.19	10/1	79.5	90
$\frac{CoMo}{Al_2O_3}$	Thiophene	603-653	1	35/1	27.6	86

$\frac{CoMo}{Al_2O_3}$	EtSH[b]	463-523	.16	5/1	92	77
MoS_2	EtSH	463-523	.16	5/1	92	77
MoS_2	EtSH	473-573	.17	5/1	83.7	75
WS_2	EtSH	473-573	.17	5/1	75.3	75
MoS_2	MeSH[c]	503-543	.22	2/1	95.8	76
WS_2	MeSH	503-583	.22	2/1	120.5	76
WS_2	MeSH	603-653	.018	56/1	24.9	This work

[a] $CoMo/Al_2O_3$ stands for a sulfided cobalt-molybdate catalyst on an alumina support.

[b] EtSH stands for ethanethiol.

[c] MeSH stands for methanethiol.

formalism (see Appendix I) since, as mentioned earlier, these are composite values. The contributions from the numerator terms of a rate expression (a rate constant and equilibrium constants) are always present, but the magnitude of the contributions from the individual adsorbate denominator terms are dependent on their surface coverages. Assuming that the enthalpies of adsorption are negative, then the denominator adsorbate equilibria terms make the activation energy more positive while the numerator adsorption equilibria terms lead to a less positive activation energy. The trend to lower activation energies with increasing hydrogen to sulfur pressure ratios seen in Table I-2 can be explained on this basis. If the heat of hydrogen adsorption is much smaller than that of the organosulfur compound, then the replacement of the adsorbed organosulfur compound by hydrogen will lead to a less positive activation energy since the denominator's contribution (which makes the activation energy more positive) is now smaller. A similar effect may occur with increasing temperature. Increasing the catalyst temperature reduces the surface concentrations of all adsorbates, thereby reducing the denominator's contribution to the activation energy. This behavior was observed by Morooka and Hamrin (87), who observed a decrease from 84 kJ/mole to

40 kJ/mole when the catalyst temperature was increased approximately 50 K. The difference in the activation energy obtained in this study, 24.9 kJ/mole, and that of Wilson and Kemball (77), 120.5 kJ/mole, when taken in this context, is not that surprising, and since the approximate reactant orders under these conditions are not their limiting values even a less positive activation energy may be observable.

The effect of product inhibition on the apparent energy of activation was also examined. Product adsorption may lead to either a less positive or more positive activation energy depending on whether it adsorbs less strongly or more strongly than the specie or species it displaces. (The argument is identical to that used earlier for hydrogen and methanethiol.) Figure I-17 shows the Arrhenius plots in the presence of 1.14×10^3 Pa (8.55 Torr) methane and 9.04×10^2 Pa (6.78 Torr) hydrogen sulfide. The reactant pressures are identical to those used to obtain the previous activation energy. The calculated values for the apparent activation energies are -11.8 kJ/mole (-2.8 kcal/mole) in the presence of methane and 8.96 kJ/mole (2.14 kcal/mole) in the presence of hydrogen sulfide. These values, especially the methane result, suggest that the product enthalpies of adsorption of are less than the methanethiol enthalpy of adsorption.

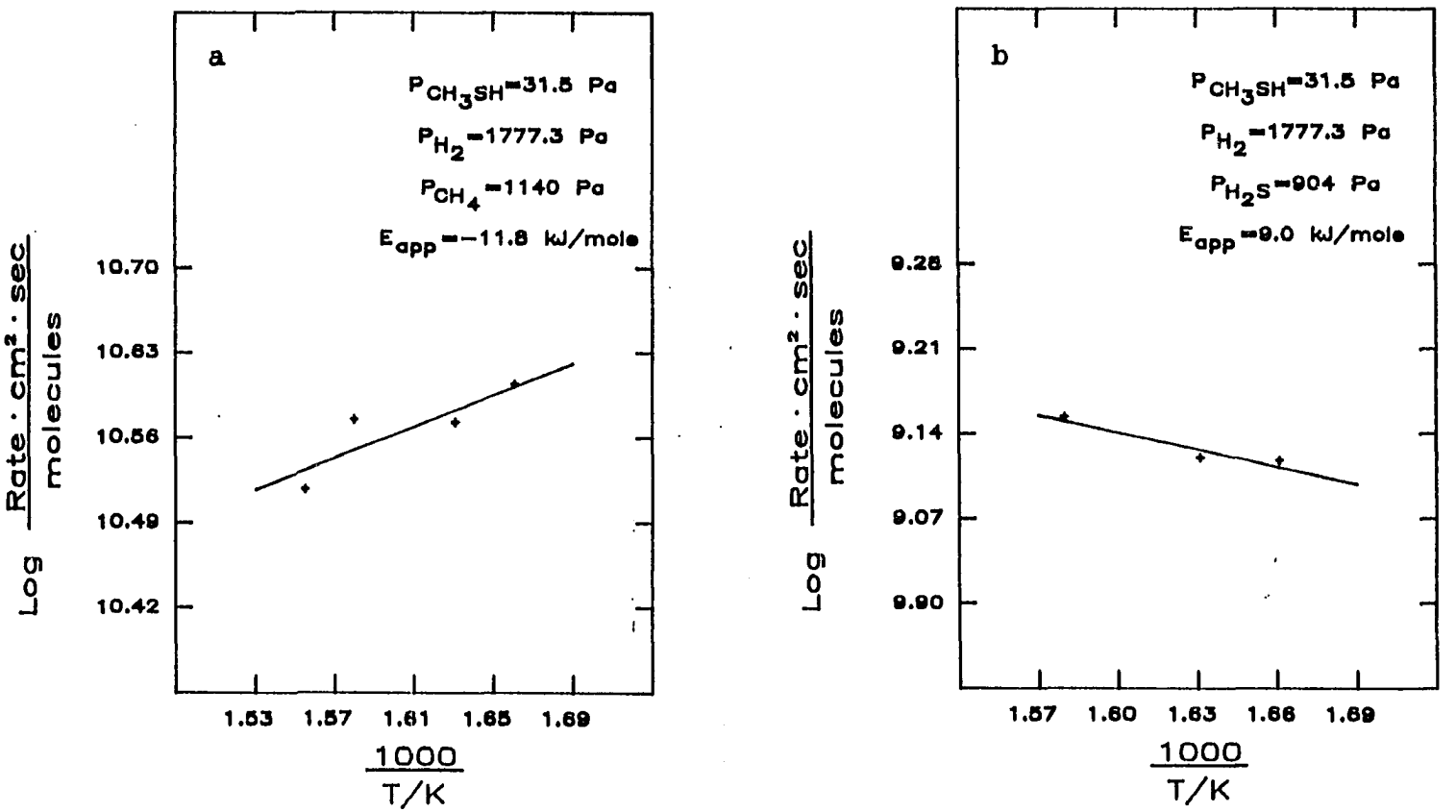

Figure I-17. Temperature dependence of the reaction in the presence of (a) methane (1140 Pa) and (b) hydrogen sulfide (904 Pa). The reactant pressures were 31.5 Pa methanethiol and 1777.3 Pa hydrogen

The rationale behind differences in activation energy with surface coverage can also be used to estimate enthalpies of adsorption (see Appendix I). This procedure requires the activation energies for when the surface is bare and when it is saturated with a single adsorbate. The adsorbate's enthalpy of adsorption is then half of the difference of these two activation energies. Conditions similar to these occur for methanethiol in this work and in the work of Wilson and Kemball (77). If it is assumed that the enthalpies of adsorption of hydrogen and methane are negligible, the apparent activation energy observed in this work, either in the presence of methane or its absence, can be used to approximate the activation energy of the HDS reaction on the bare surface. Likewise the apparent activation energy of Wilson and Kemball, 120.5 kJ/mole, can be used to approximate the activation energy of the HDS reaction on the methanethiol saturated surface. These assumptions yield a methanethiol enthalpy of adsorption of -48 or -66 kJ/mole depending on whether the activation energy on the bare surface is approximated using the apparent activation energy in the absence of any product (24.9 kJ/mole) or in the presence of methane (-11.8 kJ/mole). This methanethiol enthalpy of adsorption is probably too small since the value for adsorption on alumina

is -105 to -145 kJ/mole (91,92). (The enthalpy of adsorption of methanethiol on WS_2 or MoS_2 has not been reported.) If, rather than assuming methanethiol coverages of zero and one (as was just done), the "bare surface" and "saturated surface" activation energies were corrected for the actual methanethiol surface coverage (calculated using the parameters derived from the kinetic analysis), a better estimate of the methanethiol enthalpy of adsorption is obtained. This was done using the rate equation parameters in Table I-1. Still assuming that the enthalpies of hydrogen and methane adsorption are negligible, this yields a more reasonable value of -73 or -96 kJ/mole, again depending upon which apparent activation energy is used to approximate the activation energy for the HDS reaction on the bare surface.

CONCLUSIONS AND SUGGESTIONS FOR FUTURE RESEARCH

The relationship between the pressure of each reactant and product gas and the rate of methanethiol hydrodesulurization was observed by varying the partial pressures of these species over several orders of magnitude. The methanethiol reactant exhibited a pressure dependence that shifted from +1 at low partial pressures to -1 at higher partial pressures. The pressure dependence of hydrogen showed a shift from +1/2 to -1 with increasing partial pressure. The rate was independent of the product gases at low partial pressures but was inhibited by each product at higher partial pressures. The observed high pressure inhibition order for methane was -1, whereas an order of -2 was observed for hydrogen sulfide. The temperature dependence of the rate was also affected at high product partial pressures.

A Langmuir-Hinshelwood type mechanism and rate expression describe the data quite well. The "best fit" model describes the active site as two adjacent B type edge vacancies paired parallel to the c-axis. This "paired vacancies" site is capable of adsorbing each reactant and product gas. Hydrogen adsorption also results in the formation of a sulfhydril species. Methane is formed in the rate limiting step via the simultaneous interaction of

hydrogen and methanethiol adsorbed to the same "paired vacancies" site with hydrogen adsorbed on an adjacent sulfur atom. Hydrogen sulfide is formed in the ensuing step.

A unique feature of this mechanism is the description of the active site as paired B type vacancies. Supportive evidence for this active site description is needed, although the inability to isolate and quantify the different types of sulfur vacancies makes the acquisition of such evidence difficult. Evidence for the existence of paired vacancies, while inferential, is less difficult to obtain. As mentioned earlier, an inability of the methyl group to diffuse over the sulfur atoms of the catalyst combined with the observed formation of methyl sulfide from methanethiol would indicate the existence of adjacent vacancies. (An observation of mobile methyl groups would not disprove the existence of adjacent vacancies.) Sulfur exchange between methanethiol and isotopically labelled WS_2 during adsorption studies would provide the necessary information regarding methyl group mobility.

Several implications of this mechanism can be investigated in future studies. The sequence of steps resulting in product formation suggests that at large hydrogen-to-methanethiol ratios the added hydrogen in these products would come primarily from adsorbed hydrogen whose

origin was gas phase hydrogen. This could be checked using either deuterated methanethiol or deuterium gas. The mechanism also predicts a negative second order hydrogen dependence for extremely large hydrogen-to-methanethiol ratios and this could also be investigated.

Detailed kinetic analyses of the hydrodesulfurization of other simple organosulfur compounds would be of value; for example, the ethanethiol (C_2H_5SH) - ethenethiol (C_2H_3SH) pair. Of particular interest would be any differences resulting from the hydrogenation of the carbon-carbon bond α to the sulfur, since this is an issue of debate regarding the HDS of the heteroaromatic organosulfur compounds. (This particular experiment may be impractical due to the unstable nature of ethenethiol, although this may not be a problem with similar pairs of compounds.)

PART II. A SURVEY OF RARE EARTH SULFIDES FOR HYDRODESULFURIZATION ACTIVITY

INTRODUCTION

The sulfur oxides form a major class of gaseous pollutants. The principal man-made source of these oxides is the combustion of fuels containing organically bound sulfur. The removal of this sulfur involves catalytic hydrogenation or hydrogenolysis of the organosulfur compound to hydrocarbons and hydrogen sulfide. This process is called hydrodesulfurization, or HDS.

Currently this HDS process uses supported, cobalt promoted, molybdenum catalysts which have been either pre-sulfided or sulfided during the course of the reaction. Much of the research to date, described in the introduction of Part I, has focused on describing the structure of these "cobalt molybdate" catalysts.

The use of "dirtier" petroleum and coal feedstocks suggests the need of a newer type of catalyst (93). Pecoraro and Chianelli (93), using unsupported catalysts, have surveyed the ability of binary transition metal sulfides to catalyze the HDS reaction. They found the first row sulfides to be relatively inactive, whereas the higher activities of the second and third row metal sulfides peaked at the group VII, $VIII_a$, and $VIII_b$ catalysts. Several of the transition metal sulfides tested were not stable under reaction conditions, e.g., the osmium sulfide, OsS_2, is reduced to the metal.

McCarty and Schrader (94) have investigated the catalytic HDS activity of several Chevrel phase compounds ($M_xMo_6S_8$, M=Cu, Fe and Co). These ternary sulfides exhibited activities toward thiophene HDS comparable to unpromoted and cobalt-promoted MoS_2 model catalysts (the hydrogenation activity was much lower). The bulk Chevrel phase structure was stable under reaction conditions.

The HDS activities of the binary rare earth sulfides have not been reported. Such sulfides exist in a number of compositions (e.g., MS, M_5S_7, M_3S_4, M_2S_3 and MS_2) and phases. Several of these phases have a wide range of homogeneity. These nonstoichiometric phases may be either metal deficient (γ-$M_{3-x}S_4$) or have a deficiency and/or excess of sulfur ($MS_{2\pm x}$ and MS_{1-x}). The binary sulfides tested and reported here will be referred to as sesquisulfides. Seventeen rare earth sesquisulfides were evaluated for HDS activity using methanethiol as the organosulfur reactant. Four of the six sesquisulfides phases were tested, including the γ-phase which has a wide range of homogeneity (e.g., Nd_2S_3 or $Nd_{2.67}S_4$-Nd_3S_4). The HDS activity for the heteroaromatic thiophene was verified but not investigated in detail.

EXPERIMENTAL

Apparatus

Since many sulfides were to be analyzed, an apparatus giving a rapid evaluation of activity was desired. A catalytic microreactor, first described by Kokes et al. (95), was chosen. The apparatus, shown schematically in Figure II-1, consists of the reactor/sampling system and a gas chromatograph. The reactor/sampling system is a slightly modified (gas flow is different) version of one described by Ettre and Brenner (96). This design enables the reactant mixture to be analyzed without passage over the catalyst and provides two modes for activity evaluation: pulse and continuous. The methanethiol-hydrogen tests used the continuous mode, where the reactant gas mixture continuously flows over the catalyst and a sample of the mixture is analyzed after passage over the catalyst. The pulse mode, used in the thiophene-hydrogen test, utilizes one of the reactants (H_2) as the carrier gas and the second is added (or injected) as a pulse that is swept over the catalyst into the gas chromatograph.

The reactor and sampling systems consist of two gas sampling valves (Varian six way linear sampling valve, 57-000034-0), a dual flow crossover valve (Whitey, four way

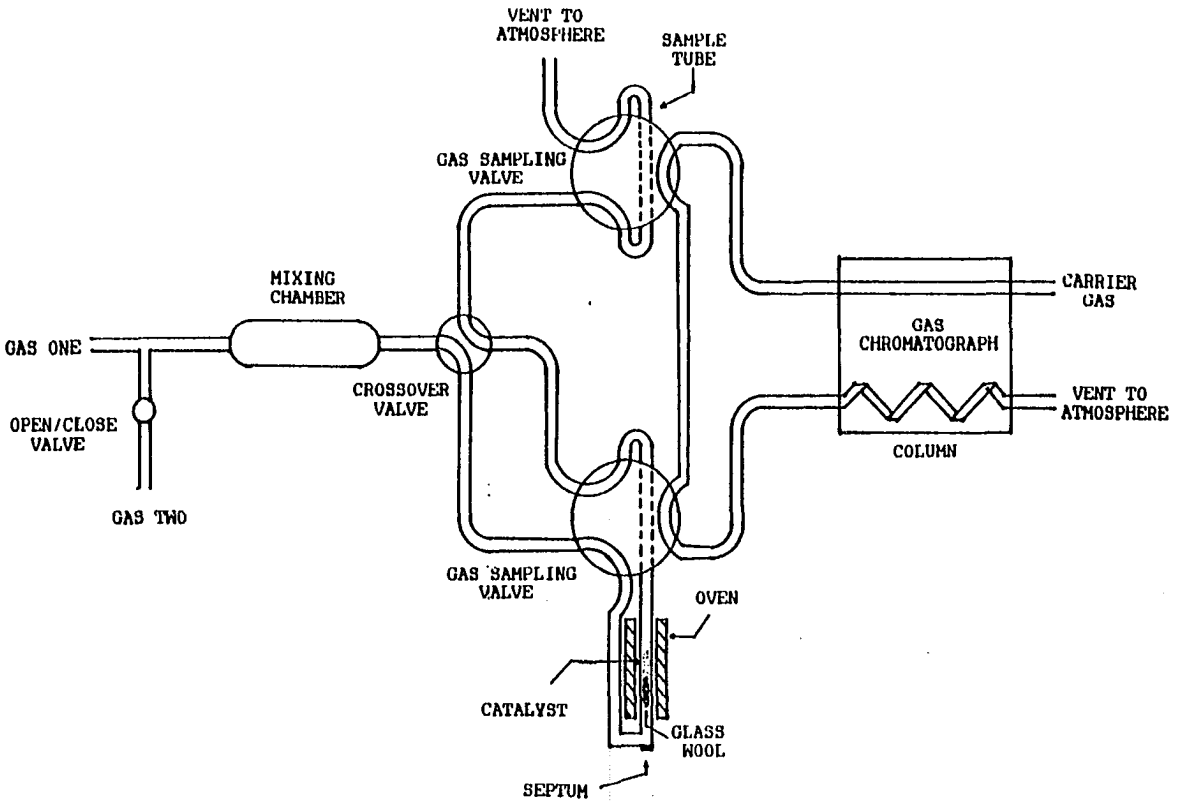

Figure II-1. Schematic of the experimental apparatus (Steady-state mode)

ball valve) and a 5 mm inner diameter pyrex reactor. Tubing between the valves, reactor, and gas chromatograph was 1/8 inch outer diameter stainless steel with swagelok connections. The swagelok connections permitted easy disassembly and rapid change of catalyst. For the thiophene experiments a general purpose blue septum was attached to one end of the reactor using a swagelok connection and liquid thiophene injected into the reactor using a 10 microliter syringe (Hamilton).

The catalyst was held in place with a quartz wool plug and heated using a tubular furnace (Mellen Co. Inc.). A chromel-alumel thermocouple either inside the reactor (stainless steel sheath) or in thermal contact with the exterior of the reactor was used to measure temperature. The temperature was read either in millivolts (Keithley 168 Autoranging Digital Multimeter), referenced to 273 K, or in degrees centigrade using a digital readout (Omega, Model 199).

For both systems studied, the gas chromatograph (Hewlett Packard, series 5750) was operated under isothermal conditions, 321 K, using a Supelco chromosil 310 teflon column (6 foot x 1/8 inch outer diameter) and a thermal conductivity detector.

Methanethiol Procedure

All catalysts were crushed and sieved to -80 +100 mesh (average particle diameter 163 μm). Each catalyst was pretreated in a flowing H_2S/H_2 mixture (14.7% H_2S balance H_2) for a minimum of two hours at a flow rate of ~ 8-12 ml/min. During this period, the thermal conductivity detector equilibrated. Calibration of the H_2S peak occurred next. This involved sampling a 1-3% H_2S in He and H_2 mixture flowing through the reactor. This percentage was attained by diluting the hydrogen sulfide-hydrogen mixture with the carrier gas, helium. Activity measurements at 653-658 Kelvin, under continuous flow conditions, were performed for three methanethiol-hydrogen mixtures (39%, 49.5%, and 57.3% CH_3SH balance H_2). Prior to taking a rate measurement, the catalyst was exposed to a flow of the reactant gas mixture (8-12 ml/min) for a minimum of 20 minutes.

The retention times for the peak maxima, relative to hydrogen sulfide, were: .6 for methane and hydrogen; 1 for hydrogen sulfide; and 6 for methanethiol (substantial tailing). Because of the overlap and tailing exhibited by three of the reactor effluent gases, only H_2S was analyzed. The relatively long retention time for methanethiol

permitted four to five samples to be taken prior to the elution of methanethiol from the first sample and this was typically done. After the last sample was taken, the catalyst was exposed to the next reaction mixture without undergoing any cleaning.

Conversion rates were calculated by dividing the amount of H_2S produced (corrected for a small background) by the residence time. The residence time is defined as the volume occupied by the catalyst divided by the flow rate of the mixture. Conversions were calculated for each sample run and the total pressure over the catalyst was assumed to be equal to ambient pressure. Since neither a systematic nor large variation in rate with reactant ratio was observed, an average activity was calculated for the mixtures tested.

Typical catalyst loadings of .1-.2 grams (volume 0.04-.08 ml) were used.

Thiophene Procedure

The procedure for thiophene was analogous to the methanethiol procedure except for changes dictated by the use of the pulse mode. These included switching to H_2 as the carrier gas, which flowed continuously over the catalyst, and the addition of the second reactant, 5 µl of liquid thiophene, via injection through the septum. A catalyst loading of 4.67 grams (volume 1.54 ml) was used.

Two product peaks were observed and identified as H_2S and an olefinic C-4 hydrocarbon. The hydrogen sulfide peak was again used to calculate conversions. The residence time was calculated assuming that the thiophene pulse traversed the catalyst in a uniform band.

A background correction for reactor activity was not required in this procedure.

Materials

All reagents were used as received. The methanethiol-hydrogen mixtures and the hydrogen sulfide-hydrogen mixture were obtained from the Linde Division, Union Carbide. Thiophene (99+%) was obtained from the Aldrich Chemical Co. Zero hydrogen was the carrier gas used in the pulse experiments.

The rare earth sulfides were obtained from the Ames Lab Materials Preparation Center. BET surface area measurements were performed on -80 +100 mesh γ-$Nd_{2.74}S_4$ using a surface-area pore-volume analyzer (Micrometrics Instruments Corp, model 2100D). This surface area, .025m^2/g, was then used to approximate the surface areas of all the catalysts listed in Table II-2, after correcting for the different densities of the sulfides. Similar particle sizes, shapes and distributions were necessarily assumed in this approximation.

RESULTS AND DISCUSSION

The principal sesquisulfides investigated for methanethiol HDS activity were γ-phase sulfides. This phase, which exhibits a wide homogeneity range, has the Th_3P_4 structure with four formula units per unit cell ($M_{12}S_{16}$). The nonstoichiometric sulfides contain the stoichiometric amount of sulfur (16 atoms per unit cell) but are deficient in metal atoms. Those sesquisulfides with an exact M_2S_3 stoichiometry ($M_{10.66}S_{16}$) have 1 1/3 metal vacancies per unit cell and are insulators. The electrical properties of this phase change continuously from insulator to metallic conductor as these vacancies are occupied. Table II-1 shows that the metallic γ-phase sulfides are generally active, whereas the γ-phase insulators are inactive. This inactivity extends to the other colored insulators, δ-Er_2S_3 and ε-Yb_2S_3, but not to the α-phase sesquisulfides, Ce_2S_3 and Dy_2S_3.

In Part I, the active site for the WS_2 catalyst was described as two adjacent edge sulfur vacancies that expose two tungsten atoms and four "dangling metal bonds". Configurations similar to this are present in all the sulfides tested, although it should be noted that these configurations are not identical to the active site in WS_2 since the coordination number and polyhedra of the rare

Table II-1. Rare earth sulfide activity for methanethiol HDS

Metal	Sulfide	Appearance	Activity
La	$\gamma La_{2.67}S_4$	Yellow	-
	$\gamma La_{2.67+x}S_4$	blue-black metallic	-
Ce	$\gamma Ce_{2.67}S_4$	purple-red	-
	αCe_2S_3	blue-black flaky	+
Pr	$\gamma Pr_{2.69}S_4$	blue-black metallic	+
	αPr_2S_3	blue-black flaky	+/-
Nd	$\gamma Nd_{2.67+x}S_4$	blue-black metallic	+
	$\gamma Nd_{2.76}S_4$	blue-black metallic	+
	$\gamma Nd_{2.86}S_4$	blue-black metallic	+
	$\gamma Nd_{2.92}S_4$	blue-black metallic	+
Gd	$\gamma Gd_{2.67}S_4$	yellow	-
Tb	$\gamma Tb_{2.67}S_4$	yellow	-
	$\gamma Tb_{2.84}S4$	blue-black metallic	+
Dy	$\gamma Dy_{2.67+x}S_4$	blue-black metallic	+
	αDy_2S_3	blue-black flaky	+
Er	δEr_2S_3	tan	+/-
Yb	εYb_2S_3	yellow	-

earth and sulfur atoms in these compounds differ from that of WS_2.

The methanethiol conversion rates for the active α- and γ-phase sulfides are shown in Table II-2; the phases appear to be of comparable activity. The series of nonstoichiometric γ-phase neodymium sulfides exhibit a small maximum in the rate for the intermediate composion $Nd_{2.76}S_4$. Since the unit cell dimensions are identical for these sulfides, this suggests a correlation between the conductivity of the sulfide and its HDS activity.

Table II-2. Methanethiol Conversion Rates of the Active Rare Earth Sulfides

Rare Earth Sulfide	Conversion Rate $10^{16} \cdot \frac{\text{molecules}}{g \cdot sec}$	$10^{14} \cdot \frac{\text{molecules}}{cm^2 \cdot sec}$
αCe_2S_3	18.25	6.42
$\gamma Pr_{2.69}S_4$	2.70	1.01
$\gamma Nd_{2.67+x}S_4$	9.24	3.62
$\gamma Nd_{2.76}S_4$	22.00	8.84
$\gamma Nd_{2.86}S_4$	9.28	3.84
$\gamma Nd_{2.92}S_4$	8.57	3.60
$\gamma Tb_{2.84}S_4$	17.24	8.12
$\gamma Dy_{2.67+x}S_4$	5.13	2.37
αDy_2S_3	11.64	5.42

Hydrodesulfurization activity toward thiophene, a more demanding test of HDS activity than methanethiol desulfurization was verified using a γ-phase neodymium sulfide of intermediate composition, $Nd_{2.74}S_4$. A conversion rate of 2.42×10^{12} molecules/cm^2·sec (6.05×10^{14} molecules/g·sec) was observed.

CONCLUSIONS AND SUGGESTIONS FOR FUTURE RESEARCH

The hydrodesulfurization activities of a number of binary rare earth sulfides, not previously reported in the literature, were examined using methanethiol as the organosulfur reactant. A correlation between activity and electrical conductivity was observed (i.e., insulators were inactive). This correlation extended to the γ phase sesquisulfides which exhibit both insulating and conducting properties.

The electrical conductivities of these sesquisulfides varies from insulating to metallic over their large homogeneity ranges. The relationship between HDS activity and electrical conductivity could be examined in detail in future research. Other rare earth sulfide compositions with large homogeneity ranges (e.g., MS_{2-x}) could also be examined.

GENERAL SUMMARY

The detailed reaction kinetics of methanethiol HDS over tungsten disulfide were described quite well using a dual site Langmuir-Hinshelwood type mechanism, which defines one adsorption site as two adjacent sulfur vacancies and the second as a neighboring sulfur atom.

The survey of rare earth sulfides for catalytic HDS activity showed that the active sulfides were conductors and the inactive sulfides were nonconductors.

REFERENCES

1. Mckinley, J. B. In "Catalysis", Emmett, P. H. Ed.; Reinhold: New York, 1957; Vol. 5, p. 405

2. Amberg, C. H. In "Proceedings Climax 1st. International Conferernce on the Chemistry and Uses of Molybdenum", Mitchell, P. C. H. Ed.; Climax Molybdenum Co. Ltd.: London, 1973; p. 180

3. Jacobsen, A. C. In "Surface Properties and Catalysis by Non-Metals", Bonnelle, J. P.; Delmon, B.; Derouane, E. Eds.; Reidel: Dordrecht, 1983; p. 305

4. Richardson, J. T. Ind. Eng. Chem. Fund. 1964, 3, 154

5. Kolboe, S.; Amberg, C. H. Can. J. Chem. 1966, 44, 2623

6. Furimsky, E.; Amberg, C. H. Can. J.Chem. 1975, 53(17), 2542

7. Ahuja, S. P.; Derrien, H. L.; Le Page, J. F. Ind. Eng. Chem., Prod. Res. Dev. 1970, 9, 272

8. Hagenbach, G.; Courty, P.; Delmon, B. J. Catal. 1977, 23, 295

9. Wivel, C.; Candia, R.; Clausen, B. S.; Mørup, S.; Topsøe, H. J. Catal. 1981, 68, 483

10. Gil, F. J.; Mendioroz, S.; Lopez Aquado, A. Bull. Soc. Chim. Belg. 1981, 90(12), 1331

11. Mitchell, P. C. H. In "Catalysis", Kemball, C.; Dowden, D. A. Eds.; The Chemical Society: London, 1981; Vol. 4, P. 175

12. Furimskey, E. Catal. Rev.-Sci. Eng. 1980, 22(3), 371

13. Ratnasamy, P.; Sivasanker, S. Catal. Rev.-Sci. Eng. 1980, 22(3), 401

14. Grange, P. Catal. Rev.-Sci. Eng. 1980, 21(1), 135

15. Massoth, F. E. Adv. Catal. 1978, 27, 266

16. Wivel, C.; Clausen, B. S.; Candia, R.; Mørup, S.; Topsøe, H. J. Catal. 1984, 87, 497

17. Lipsch, J. M. J. G.; Schuit, G. C. A. J. Catal. 1969, 15, 163, 228, 243

18. Voorhoeve, R. J. H.; Stuiver, J. C. M. J. Catal. 1971, 23, 228, 243

19. Farragher, A. L.; Cossee, P. In "Proceedings 5th. International Congress on Catalysis", Hightower, J. W Ed.; North-Holland: Amsterdam, 1973; Vol. 1A, p. 1301

20. Schuit, G. C. A. Intl. J. Quant. Chem. 1977, 12(suppl.2), 43

21. Delmon, B. In "Proceedings Climax 3rd. International Conference on the Chemistry and Uses of Molybdenum", Barry, H. F.; Mitchell, P. C. H. Eds.; Climax Molybdenum Co.: Ann Arbor, 1979; p. 73

22. Hagenbach, G.; Courty, P.; Delmon, B. J. Catal. 1973, 31, 264

23. Delmon, B. Bull. Soc. Chim. Belg. 1979, 88(12), 979

24. Massoth, F. E. J. Catal. 1975, 36, 164

25. Walton, R. A. J. Catal. 1976, 44, 335

26. Clausen, B. S.; Topsøe, H.; Candia, R.; Villadsen, J.; Lengeler, B.; Als-Nielsen, J.; Christensen, F. J. Phys. Chem. 1981., 85, 3868

27. Kohatsu, I.; Blakely, D. W.; Harnsperger, H. F. In "Synchrotron Radiation Research", Winick, H.; Doniach, S. Eds.; Plenum: New York, 1980; P. 417

28. Parham, T. G.; Merril, R. R. J. Catal. 1984, 85, 295

29. Delmon, B. Am. Chem. Soc., Div. Petro. Chem., Prepr. 1977, 22, 503

30. Topsøe, N.; Topsøe, H. Bull. Soc. Chim. Belg. 1979, 90(12), 1311

31. Gajardo, P.; Mathieux, A.; Grange, P.; Delmon, B. Appl. Catal. 1982, 3, 347

32. Massoth, F. E.; MuraliDhar, G. In "Proceedings Climax 4th. International Conference on the Chemistry and Uses of Molybdenum", Barry, H. F.; Mitchell, P. C. H. Eds.; Climax Molybdenum Co.: Ann Arbor, 1982; p. 343

33. Topsøe, H.; Clausen, B. S.; Candia, R.; Wivel, C.; Mørup, S. Bull. Soc. Chim. Belg. 1979, 90(12), 1190

34. Topsøe, H. In "Surface Properties and Catalysis by Non-Metals", Bonnelle, J. P.; Delmon, B.; Derouane, E. Eds.; Reidel: Dordrecht, 1983; p.329

35. Weisser, O.; Landa, S. In :"Sulphide Catalysts, Their Properties, and Applications", Pergamon: New York, 1973; p. 210

36. Vrinat, M. L. Appl. Catal. 1983, 6, 137

37. Satterfield, C. N.; Roberts, G. W. A. I. Ch. E. J. 1968, 14, 159

38. Chakroborty, P.; Kar, A. K. Ind. Eng. Chem., Proc. Des. Dev. 1978, 17, 252

39. Kilanowski, D. R.; Gates, B. C. J. Catal. 1980, 62, 70

40. Broderick, D. H.; Gates, B. C. A. I. Ch. E. J. 1981, 27, 663

41. Devanneaux, J.; Maurin, J. J. Catal. 1981, 69, 202

42. Dhainaut, E.; Gachet, C.; de Mourges, L. C. R. Hebd. Seances Acad. Sci. Ser. C 1979, 288,339

43. Blake, M. R.; Eyre, M.; Moyes, R. B.; Wells, P. B. Stud. Surf. Sci. Catal. 1981, 7A, 591

44. Vrinat, M. L.; De Mourges, L. J. Chim. Phys. 1982, 79(1), 45

45. Kawaguchi, Y.; Dalla Lana, I. G.; Otto, F. D. Can. J. Chem. Eng. 1978, 56, 65

46. Williamson, J. G.; John, C. S.; Kemball, C. J. Chem. Soc., Farad. Trans. I 1980, 76(6), 1366

47. Zdrazil, M. Appl. Catal. 1982, 4, 107

48. Owens, P. J.; Amberg, C. H. Adv. Chem. Ser. 1961, 33, 181

49. Kraus, J.; Zdrazil, M.; React. Kinet. Catal. Lett. 1977, 6(4), 475

50. Daly, F. P. J. Catal. 1978, 51, 221

51. Houlla, M.; Nag, N. K.; Sapre, A. V.; Broderick, D. H.; Gates, B. C. A. I. Ch. E. J. 1978, 24, 1015

52. Mirza, M. L.; Campbell, K. C.; Thomson, S. J.; Webb, G. Radiochem. Radioanal. Lett. 1982, 54(4),249

53. Gachet, C. G.; Dhainaut, E.; de Mourges, L.; Candy, J. P.; Fouilloux, P. Bull. Soc. Chim. Belg. 1979, 90(12), 1279

54. Stevens, G. C.; Edmonds, T. In "Proceedings Climax 2nd. International Conference on the Chemistry and Uses of Molybdenum", Mitchell, P. C. H.; Seaman, A. Eds.; Climax Molybdenum Co.: London, 1977; p. 155

55. Chianelli, R. R.; Tauster, S. J. J. Catal. 1981, 71(1),228

56. Bahl, P. O.; Evans, E. L.; Thomas, J. M. Proc. R. Soc. Lond. Ser. A 1968, 306, 53

57. Tauster, S. J.: Pecoraro, T. A.; Chianelli, R. R. J. Catal. 1980, 63, 515

58. Bachelier, J.; Tilliette, M. J.; Duchet, J. C.; Cornet, P. J. Catal. 1982, 76, 300

59. Uchytil, J.; Beranek, L.; Zahradnikova, H.; Kraus, M. Appl. Catal. 1982m 4, 233

60. Jung, H. J.; Schmitt, J. L.; Ando, H. In "Proceedings Climax 4th. International Conference on the Chemistry and Uses of Molybdenum", Barry, H. F.; Mitchell, P. C. H. Eds.; Climax Molybdenum Co.: Ann Arbor, 1982; p. 246

61. Valyon, J.; Hall, W. K. J. Catal. 1983, 84, 216

62. Zmierczak, W.; MuraliDhar, G.; Massoth, F. E. J. Catal. 1982, 77, 432

63. Topsøe, N.; Topsøe, H J. Catal. 1982, 75, 354

64. Burch, R.; Collins, A. In "Proceedings Climax 4th. International Conference on the Chemistry and Uses of Molybdenum", Barry, H. F.; Mitchell, P. C. H. Eds.; Climax Molybdenum Co.: Ann Arbor, 1982; p. 246

65. Houlla, M. Broderick, D. H.; Sapre, A. V.; Nag, N. K.; deBeer, V. H. J.; Gates, B. C.; Kwart, H. J. Catal. 1980, 61, 523

66. Kilanowski, D. R.; Teeuwen, H.; deBeer, V. H. J.; Gates, B. C.; Schuit, G. C. A.; Kwart, H. J. Catal. 1978, 55, 129

67. Kwart, H.; Schuit, G. C. A.; Gates, B. C. J. Catal. 1980, 61, 128

68. Wright, C. J.; Fraser, D.; Moyes, R. B.; Wells, P. B. Appl. Catal. 1981, 1,49

69. Wright, C. J,; Sampson, C.; Fraser, D.; Moyes, R. B.; Wells, P. B.; Riekel, C. J. Chem. Soc., Farad. Trans. I 1980, 76(7), 1585

70. Maternova, J. Appl. Catal. 1983, 6(1), 61

71. Eischens, R. P.; Pliskin, W. A.; Low, M. J. D. J. Catal. 1962, 1, 180

72. Kokes, R. J. Catal. Rev. 1972, 6, 1

73. Fraser, D.; Moyes, R. B.; Wells, P. B. Stud. Surf. Sci. Catal. 1981, 7B, 1424

74. Vasudevan, S.; Thomas, J. M.; Wright, C. J.; Sampson, C. J. Chem. Soc., Chem. Commun. 1982, (7), 418

75. Wilson, R. L.; Kemball, C.; Galwey, A. K. Trans. Farad. Soc. 1962,58, 583

76. Kieran, P.; Kemball, C. J. Catal. 1965, 4, 380

77. Wilson, R. L.; Kemball, C. J. Catal. 1964, 3, 426

78. Tanaka, K.; Okuhara, T. Catal. Rev.-Sci. Eng. 1977, 15(2), 249

79. Boudart, M. and Djega-Mariadassou, G. In "Kinetics of Heterogenous Catalytic Reactions", Princeton University Press: Princeton, 1984; p.94

80. Adams, D. M. In "Inorganic Solids", Wiley: New York, 1974; p.85,230

81. Kalechite, I. V. Discussion following Paper 94 In "Proceedings 5th. International Congress on Catalysis", Hightower, J. W. Ed.;North-Holland: Amsterdam, 1973; Vol. 1A

82. Kuehn, C. G. and Isied, S. S. Prog. Inorg. Chem. 1980, 27, 153

83. Rakowski-Dubois, M., Van Derveer, M. C., DuBois, D. L., Haltiwanger, R. C. and Miller, W. K. J. Amer. Chem. Soc. 1980, 102(25), 7456

84. Connelly, N. G. and Dahl, L. F. J. Amer. Chem. Soc. 1970, 92(25), 7470

85. Siegal, S J. Catal. 1973, 30. 139

86. Namba, S. and Aonuma, T. Kogyo Kagaku Zasshi 1971, 74(7), 1324

87. Morooka, S. and Hamrin Jr., C. E. Chem. Eng. Sci. 1977, 32, 125

88. Lee, H. C. and Butt, J. B. J. Catal. 1977, 49, 320

89. Chakraborty, P. and Kar, a. K. Ind. Eng. Chem. Proc. Des. Dev. 1978, 17(3), 252

90. Kieran, P. and Kemball, C. J. Catal. 1965, 4, 394

91. Glass, R. W. and Ross, R. A. J. Phys. Chem. 1973, 77(21), 2576

92. Meyer, C. and Bastick, J. Bull. Soc. Chim. Fr. 1979, 11-12(Pt. 1), 463

93. Pecoraro, T. A. and Chianelli, R. R. J. Catal. 1981, 67, 430

94. McCarty, K. F. and Schrader, G. L. Ind. Eng. Chem. Prod. Res. Dev. 1984, 23, 519

95. Kokes, R. J., Tobin, H. and Emmett, P. H. J. Am. Chem. Soc. 1955, 77, 5860

96. Ettre, L. S. and Brenner, N. J. Chromatog. 1960, 3, 524

ACKNOWLEDGEMENTS

I wish to thank Dr. Robert S. Hansen for his support, understanding and assistance during my graduate student career. The phrase "Maxima enim est hominum semper patientia virtus", attributed to Cato, best describes a quality of Dr. Hansen's that was especially appreciated.

I also wish to acknowledge the friends I found here in Ames for making my stay a not unpleasant one. The assistance provided by the staff and support groups of Ames Lab is also appreciated.

Finally, I wish to thank my parents and fellow siblings for their encouragement and moral support.

APPENDIX I. THE LANGMUIR-HINSHELWOOD FORMALISM

The Langmuir-Hinshelwood kinetic model assumes the rate limiting step involves the reaction of two adsorbed species and that the reactant adsorption steps and other surface reaction steps prior to the rate limiting step have reached equilibrium. The rate expression using the Langmuir-Hinshelwood formalism is derived below for the mechanism shown in equations AI-1 to AI-3. In these equations ★

$$A(g) + \star \overset{K_A}{\rightleftharpoons} A\star \qquad \text{(AI-1)}$$

$$B(g) + \star \overset{K_B}{\rightleftharpoons} B\star \qquad \text{(AI-2)}$$

$$A\star + B\star \overset{k}{\longrightarrow} AB(g) + 2\star \qquad \text{(AI-3)}$$

represents a surface site, A★ and B★ the adsorbed reactants and A, B, and AB the reactant and product gases. K_A and K_B are the equilibrium constants for the adsorption processes while k is the rate constant of the rate limiting step. The rate is expressed by

$$\text{rate} = k[A\star][B\star] \qquad \text{(AI-4)}$$

where [A★] and [B★] are the fraction of surface sites occupied by the adsorbed reactants A and B. The establishment of equilibrium in the steps prior to the rate limiting step implies the following relationships:

$$[A^*] = K_A P_A [^*] \qquad \text{(AI-5)}$$

$$[B^*] = K_B P_B [^*] \qquad \text{(AI-6)}$$

where $[^*]$ is the fraction of sites unoccupied. These two relationships together with the conservation of surface sites ($1=[^*]+[A^*]+[B^*]$) allows the fraction of unoccupied sites to be expressed in pressure dependent terms only.

$$1 = [^*]+[A^*]+[B^*] \qquad \text{(AI-7)}$$

$$1 = [^*](1+K_A P_A+K_B P_B) \qquad \text{(AI-8)}$$

$$[^*] = \frac{1}{(1+K_A P_A+K_B P_B)} \qquad \text{(AI-9)}$$

Using equations AI-5, AI-6, and AI-9 the rate expression, equation AI-4 becomes

$$\text{rate} = \frac{kK_A P_A K_B P_B}{(1+K_A P_A+K_B P_B)^2} \qquad \text{(AI-10)}$$

It is apparent from this expression that at a low reactant pressure (e.g., $K_A P_A << 1+K_B P_B$) the reactant order is +1. As the reactant pressure increases (keeping everything else constant) this order decreases to zero and finally to -1 at high pressures ($K_A P_A >> 1+K_B P_B$). The negative reactant order is a manifestation of the competitive adsorption process (both reactants can adsorb at the same site). Using this and analogous procedures, rate expressions can be derived

for any postulated mechanism. The form and complexity of such expressions depend on the mechanism and its assumptions (e.g., does product adsorption occur or are there steps involving the reactants after adsorption but prior to the rate limiting step). One result of the added complexity is the possible replacement of K_A with a product of equilibrium constants so that this new parameter is no longer associated with a single step in the mechanism.

The temperature dependence of these expressions is contained within the rate constant ($k=Aexp(-E/RT)$) and the adsorption equilibrium constants ($K_{A,B}=A_{A,B}exp(-\Delta H_{A,B}/RT)$, where $\Delta H_{A,B}$ is the enthalpy of chemisorption and is negative. Arrhenius type plots (log rate vs. 1/RT) are used to obtain the temperature dependence and apparent activation energies. The mathematical expression for the apparent activation energy, E_{app}, is shown in equation AI-11. It is

$$E_{app} = E+\Delta H_A+\Delta H_B-2\frac{\Delta H_A K_A P_A+\Delta H_B K_B P_B}{(1+K_A P_A+K_B P_B)} \qquad \text{(AI-11)}$$

obvious from this equation that the observed activation energy is dependent on the pressure conditions and is not necessarily independent of temperature (i.e., this expression still contains the temperature dependent terms K_A and K_B). Two limiting cases exist where this is not true;

(1) when the surface is saturated with one reactant, e.g., $K_A P_A >> 1+K_B P_B$, and (2) when the surface is essentially bare, $1 >> K_A P_A + K_B P_B$. Under these conditions, the apparent activation energies have the form:

Case I $(K_A P_A >> 1+K_B P_B)$

$$E_{app} = E + \Delta H_B - \Delta H_A \qquad \text{(AI-12)}$$

Case II $(1 >> K_A P_A + K_B P_B)$

$$E_{app} = E + \Delta H_A + \Delta H_B \qquad \text{(AI-13)}$$

It is apparent from the limiting cases that the observed activation energy is dependent on the relative magnitudes of the true activation energy and the enthalpies of chemisorption. If, for instance, $|\Delta H_A + \Delta H_B| > E$, then the observed activation energy is negative in Case II (recall that the enthalpies of chemisorption are negative).

These two limiting cases can be combined to estimate enthalpies of adsorption. In the above example, the enthalpy of adsorption of reactant A, ΔH_A, is determined in the following manner:

$$E_{app}(\text{case II}) - E_{app}(\text{case I}) = 2\Delta H_A \qquad \text{(AI-14)}$$

$$\Delta H_A = [E_{app}(\text{case II}) - E_{app}(\text{case I})]/2 \qquad \text{(AI-14a)}$$

APPENDIX II. DERIVATION OF THE SINGLE VACANCY RATE EXPRESSION

The proposed reaction sequence for the single vacancy per site mechanism is reproduced below and assumes equilibrium is established for those steps prior to the rate limiting step, equation I-22.

$$H_2 + *_b \langle===\rangle H_2*_b \qquad \text{(I-18)}$$

$$H_2*_b + S \langle===\rangle H*_b + HS \qquad \text{(I-19)}$$

$$H*_b + S \langle===\rangle *_b + HS \qquad \text{(I-20)}$$

$$CH_3SH + *_b + S \langle===\rangle CH_3S*_b + HS \qquad \text{(I-21)}$$

$$CH_3S*_b + HS + *_bH \text{ ---}\rangle CH_4 + HS*_b + S + *_b \qquad \text{(I-22)}$$

$$HS*_b + HS \text{ ---}\rangle H_2S + S + *_b \qquad \text{(I-23)}$$

The Langmuir-Hinshelwood formalism allows the following expressions to be derived

$$[H_2*_b] = K_{18}P_{H_2}[*_b] \qquad \text{(AII-1)}$$

$$[H*_b] = K_{19}[H_2*_b][S]/[HS] \qquad \text{(AII-2)}$$

$$[HS] = K_{20}[H*_b][S]/[*_b] \qquad \text{(AII-3)}$$

(These last two expressions can be rearranged to yield equations AII-2a and AII-3a.)

$$[H^*_b] = (K_{18}K_{19}/K_{20})^{1/2}P_{H_2}^{1/2}[^*_b] \qquad \text{(AII-2a)}$$

$$[HS] = (K_{18}K_{19}K_{20})^{1/2}P_{H_2}^{1/2}[S] \qquad \text{(AII-3a)}$$

$$[CH_3S^*_b] = K_{21}P_{CH_3SH}[^*_b][S]/[HS] \qquad \text{(AII-4)}$$

$$= \frac{K_{21}P_{CH_3SH}[^*_b]}{(K_{18}K_{19}/K_{20})^{1/2}P_{H_2}^{1/2}} \qquad \text{(AII-4a)}$$

A similar expression can be derived for the fractional coverage of HS^*_b based on the stiochiometry of the reaction (equal rates of product formation).

$$k_{22}[CH_3S^*_b][^*_bH][HS] = k_{23}[HS^*_b][HS] \qquad \text{(AII-5)}$$

$$[HS^*_b] = (k_{22}/k_{23})[CH_3S^*_b][^*_bH] \qquad \text{(AII-6)}$$

$$= \frac{k_{22}K_{21}}{k_{23}K_{20}}P_{CH_3SH}[^*_b] \qquad \text{(AII-6a)}$$

These expressions and those for the conservation of surface sites, equations AII-7 and AII-8, allow the rate expression

$$1 = [S]+[HS] \qquad \text{(AII-7)}$$

$$1 = [^*_b]+[H_2^*_b]+[H_2^*_bH_2]+[CH_3S^*_b]+[HS^*_b] \qquad \text{(AII-8)}$$

to be derived, equation AII-9.

$$\text{rate} = \frac{aP_{CH_3SH}P_{H_2}^{1/2}}{\left(1+bP_{H_2}^{1/2}+cP_{H_2}+d\frac{P_{CH_3SH}}{P_{H_2}^{1/2}}+eP_{CH_3SH}\right)^2} \cdot \frac{1}{\left[1+fP_{H_2}^{1/2}\right]} \qquad \text{(AII-9)}$$

where $a = k_{22}K_{21}(K_{18}K_{19}/K_{20})^{1/2}$

$b = (K_{18}K_{19}/K_{20})^{1/2}$

$c = K_{18}$

$d = K_{21}/(K_{18}K_{19}K_{20})^{1/2}$

$e = k_{22}K_{21}/(k_{23}K_{20})$

$f = (K_{18}K_{19}K_{20})^{1/2}$

As mentioned in the text, the $\bar{H}^*_b$ and HS^*_b terms have a negligible surface concentration and their pressure dependencies are not included in equation I-17, i.e. b=0 and e=0. Thus equation AII-9 becomes, after dropping these terms,

$$\text{rate} = \frac{aP_{CH_3SH}P_{H_2}^{1/2}}{\left(1+bP_{H_2}+c\frac{P_{CH_3SH}}{P_{H_2}^{1/2}}\right)^2} \cdot \frac{1}{\left[1+dP_{H_2}^{1/2}\right]} \qquad \text{(AII-10)}$$

where $a = k_{22}K_{21}(K_{18}K_{19}/K_{20})^{1/2}$

$$b = K_{18}$$

$$c = K_{21}/(K_{18}K_{19}K_{20})^{1/2}$$

$$d = (K_{18}K_{19}K_{20})^{1/2}$$

The derived expression, AII-10, is now identical to equation I-17. (P_{SH} replaces P_{CH_3SH} in Part I of the thesis.)

APPENDIX III. DERIVATION OF THE PAIRED VACANCIES RATE EXPRESSION

The proposed reaction sequence for the paired vacancies site mechanism is reproduced below and assumes equilibrium is established for those steps prior to the rate limiting step, equation I-34.

$$H_2 + *_b \langle===\rangle H_2*_b \qquad (I-24)$$

$$H_2 + *_bH_2 \langle===\rangle H_2*_bH_2 \qquad (I-25)$$

$$H_2*_b + S \langle===\rangle H*_b + HS \qquad (I-26)$$

$$H*_b + S \langle===\rangle *_b + HS \qquad (I-27)$$

$$H_2*_bH_2 + S \langle===\rangle H_2*_bH + HS \qquad (I-28)$$

$$H_2*_bH + S \langle===\rangle H_2*_b + HS \qquad (I-29)$$

$$CH_3SH + S \langle===\rangle CH_3S*_b + HS \qquad (I-30)$$

$$CH_3SH + *_bH + S \langle===\rangle CH_3S*_bH + HS \qquad (I-31)$$

$$CH_3SH + *_bH_2 + S \langle===\rangle CH_3S*_bH_2 + HS \qquad (I-32)$$

$$CH_3SH + CH_3S*_b + S \langle===\rangle CH_3S*_bSCH_3 + HS \qquad (I-33)$$

$$CH_3S*_bH + HS \longrightarrow CH_4 + HS*_b + S \qquad (I-34)$$

$$HS*_b + HS \longrightarrow H_2S + *_b + S \qquad (I-35)$$

The Langmuir-Hinshelwood formalism allows the following expressions to be derived

$$[H_2{*_b}] = K_{24}P_{H_2}[{*_b}] \qquad \text{(AIII-1)}$$

$$[H_2{*_b}H_2] = K_{24}K_{25}P_{H_2}^2[{*_b}] \qquad \text{(AIII-2)}$$

$$[H{*_b}] = K_{26}[H_2{*_b}][S]/[HS] \qquad \text{(AIII-3)}$$

$$[HS] = K_{27}[H{*_b}][S]/[{*_b}] \qquad \text{(AIII-4)}$$

(These last two steps can be rearranged to give equations AIII-3a and AIII-4a.)

$$[H{*_b}] = (K_{24}K_{26}/K_{27})^{1/2}P_{H_2}^{1/2} \qquad \text{(AIII-3a)}$$

$$[HS] = (K_{24}K_{26}K_{27})^{1/2}P_{H_2}^{1/2} \qquad \text{(AIII-4a)}$$

$$[H_2{*_b}H] = K_{28}[H_2{*_b}H_2][S/[HS] \qquad \text{(AIII-5)}$$

$$= \frac{K_{24}K_{25}K_{28}}{(K_{24}K_{26}K_{27})^{1/2}} \cdot P_{H_2}^{3/2}[{*_b}] \qquad \text{(AIII-5a)}$$

$$[CH_3S{*_b}] = K_{30}P_{CH_3SH}[{*_b}][S]/[HS] \qquad \text{(AIII-6)}$$

$$= \frac{K_{30}P_{CH_3SH}\,[{*_b}]}{(K_{24}K_{26}K_{27})^{1/2}P_{H_2}^{1/2}} \qquad \text{(AIII-6a)}$$

$$[CH_3S{*_b}H] = K_{31}P_{CH_3SH}[{*_b}H][S]/[HS] \qquad \text{(AIII-7)}$$

$$= (K_{31}/K_{27})P_{CH_3SH}[{*_b}] \qquad \text{(AIII-7a)}$$

$$[CH_3S*_bH_2] = K_{32}P_{CH_3SH}[*_bH_2][S]/[HS] \quad \text{(AIII-8)}$$

$$= \frac{K_{32}K_{24}P_{CH_3SH}P_{H_2}^{1/2}[*_b]}{(K_{24}K_{26}K_{27})^{1/2}} \quad \text{(AIII-8a)}$$

$$[CH_3S*_bSCH_3] = K_{33}[CH_3S*_b][S]/[HS] \quad \text{(AIII-9)}$$

$$= \frac{K_{33}K_{30}P_{CH_3SH}^2[*_b]}{K_{24}K_{26}K_{27}P_{H_2}} \quad \text{(AIII-9a)}$$

The stoichiometry of the reaction implies the relationships shown in equations AIII-10, AIII-11 and AIII-11a.

$$k_{34}[CH_3S*_bH][HS] = k_{35}[HS*_b][HS] \quad \text{(AIII-10)}$$

$$[HS*_b] = (k_{34}/k_{35})[CH_3S*_bH] \quad \text{(AIII-11)}$$

$$= \frac{k_{34}K_{31}}{k_{35}K_{27}}P_{CH_3SH}[*_b] \quad \text{(AIII-11a)}$$

These expressions and those for the conservation of surface sites, equations AIII-12 and AIII-13, allow the rate

$$1 = [S]+[HS] \quad \text{(AIII-12)}$$

$$1 = [*_b]+[H_2*_b]+[H_2*_bH_2]+[CH_3S*_b]+$$

$$[CH_3S*_bH_2]+[CH_3S*_bSCH_3]+[HS*_b] \quad \text{(AIII-13)}$$

expression, equation AIII-14, to be derived.

$$\text{rate} = \frac{aP_{CH_3SH}P_{H_2}^{1/2}}{\left(1+bP_{H_2}+cP_{H_2}^2+d\frac{P_{CH_3SH}}{P_{H_2}^{1/2}}+eP_{CH_3SH}P_{H_2}^{1/2}+f\frac{P_{CH_3SH}^2}{P_{H_2}}\right)} \cdot \frac{1}{\left[1+gP_{H_2}^{1/2}\right]}$$

(AIII-14)

where $a = k_{34}K_{31}(K_{24}K_{26}/K_{27})^{1/2}$

$b = K_{24}$

$c = K_{24}K_{25}$

$d = K_{30}/(K_{24}K_{26}K_{27})^{1/2}$

$e = K_{32}K_{24}^{1/2}/(K_{26}K_{27})^{1/2}$

$f = K_{33}K_{30}/(K_{24}K_{26}K_{27})$

$g = (K_{24}K_{26}K_{27})^{1/2}$

As mentioned in the text, the H^*_b species has a negligible surface concentration, $[H^*_b]=0$, so its pressure dependent term was not included in equation AIII-14. Likewise, those species having only a single hydrogen atom occupying a vacancy (half of the adsorption site), $H_2{}^*_bH$ and $CH_3S^*_bH$, are also not included. This derived expression is identical to equation I-36. (P_{SH} replaces P_{CH_3SH} in Part I of the thesis.)